ISSN: 2753-7919
British Journal of Healthcare and Medical Research; Vol. 13 No. 04 (2026) (340-397)
https://doi.org/10.14738/bjhr.1304.11974

Mesh Materials Used for Hernia Repair: Why Do They Shrink?

Chaojing Li[1], Wan Li[1], Yijia Sun[1], Gaétan Brochu[2], Eric Philippe[2], Shanshan Wang[2,3], Linli Miao[1], Jean Michel Bourget[2], Valérie Courval[2], Léonic Bouvet[2], Ze Zhang[2], Lucie Germain[2], Lu Wang[1], Robert Guidoin[2]

1. Key Laboratory of Textile Science and Technology, Ministry of Education and College of Textiles, Donghua University, Shanghai, China
2. Department of Surgery, Faculty of Medicine, Université Laval and Axe de Médecine Régénératrice, Centre de Recherche du CHU de Québec – Université Laval, Québec (QC), Canada
3. Department of Ophthalmology, Ruijin Hospital, School of Medicine, Shanghai Jiao Tong University, Shanghai, China

Abstract: Eleven hernia repair meshes implanted for up to 4 years were harvested at reoperation: 9 recurrences, 1 infection, and 1 infection associated with a fistula. They were made of polypropylene (PP) fabric and/or expanded polytetrafluoroethylene (ePTFE). The devices shrank considerably from 12 to 53% with heavy fibrotic embedding. This shrinkage occurred due to the contraction of the fibrotic tissues that penetrated through the materials and encroached all the polymer structures. The level of inflammation was aggravated in the case of oxidation of the external surface of the PP fibers. Multiple flaking led to detachment of PP particles. In addition, the collagen bundles in the scar tissue did not show any waviness, and thus could be considered as responsible for the lack of elasticity of the encapsulating tissues. Furthermore, particles from the ePTFE structures were occasionally identified dispersed in peri-implant tissues. Despite the plethora of devices commercially available, there is still no consensus about the most appropriate one. Future hernia mesh devices should reduce fibrotic encapsulation and encourage the formation of wavy collagen fibers and thus the elasticity of the encapsulation, which would prevent mesh shrinkage and lead to the lifelong rehabilitation of the patient. The search for smart materials and novel designs must be undertaken. Future devices should demonstrate adequate long-term biostability without ignoring the importance of biocompatibility.

Keywords: hernia, polypropylene mesh, shrinkage, embedding, degradation, scar tissue, inflammation

INTRODUCTION

Hernia occurs when part of the intestine or other tissues protrudes a weak spot in the abdominal wall, often in the groin. More than half a million patients are operated in the USA and about 20 million inguinal hernia surgeries operated worldwide every year [1, 2]. Surgery is known to relieve pain and prevent strangulation of the intestine or other organs, which can be life-threatening. The conventional surgery consists of an incision over the site of the hernia, returning the protruding tissue to the abdominal cavity, and removing the hernia sac. The surrounding muscles are sutured to close the defect. This tension-based technique has been known to be associated with high rates of reoccurrence [3]. The implantation of a surgical mesh, also called a patch, can eliminate the tension, promotes a

fast recovery, allows tissue in growth, and significantly reduces reoccurrence [4, 5]. A plethora of devices were developed over the last few decades, resulting in a tremendous increase in both the number and the types of prosthetic mesh devices [6-11]. These include meshes made from monofilament polypropylene (PP), multifilament polyethylene terephthalate (PET), and expanded polytetrafluoroethylene (ePTFE) [1, 12]. The composite patches typically consist of a synthetic polymer mesh combined with an absorbable coating on the filament. Composite barrier patches are also available, in which a synthetic mesh can be combined with a permanent or absorbable adhesion barrier layer. The plethora of commercially available meshes is a clear-cut indication of the lack of consensus in selecting the most appropriate device for the treatment of the patients [6, 13, 14]. The recurrence of hernia is considered to vary between 10 and 20% [15]. There is a lack of precise information about the performance of each type of mesh in the absence of randomized multicentre trials [7, 16, 17]. More attention shall be paid to investigate the explanted devices after adverse events, to discriminate between patient related failures, device related adverse events, and eventually mishandling of the devices [18, 19]. Retrieved explants should be carefully analyzed following clinical reporting, more specifically through such regulatory set up as MAUDE, in the USA [20]. Over the last decade, FDA recalled several devices [21, 22]. Ideally, any device implanted in the body requires a lifelong assessment, ideally in the absence of any adverse event.

Patient evaluation before the surgery is of critical importance. The concept that one mesh fits all patients cannot be tolerated. The surgeon shall select a device amongst what is available on the shelf. Mesh weight, pore size, permanent or resorbable represent the vocabulary understood by the surgeons [23-25]. Unfortunately, there is a mismatch with the vocabulary of the manufacturers together with the engineers, who understand tensile strength, suture pull out strength, creeping characteristics, to name a few [26, 27]. Surgeons and engineers are at odd. A sound understanding of the patients' requirements requires a common language to bridge the communication between surgeons and engineers. Klinge and Deeken pioneered the sound classifications over the last decade [18, 27, 28, 29]. Pore size, thickness, and weight are the principal words that help advance the characterization of the hernia meshes [23, 30, 31]. We hereby report a series of analyses of hernia mesh explants, consisting of naked-eye observations, pathological investigations, and chemical and physical characterizations. Our ambitious undertaking aims to establish a sound dialogue between doctors and engineers for the benefit of patients.

MATERIALS AND METHODS

Explants

The CHU-Université Laval in Québec City, Québec, Canada, is a referral center for reoperations on patients who have received hernia meshes and subsequently experienced adverse events, such as hernia recurrences with or without infection. Eleven explanted ventral meshes of large sizes up to 30 cm × 20 cm were used for this series of investigation, including nine cases without infection, one case with infection, and one case with infection associated with a fistula (Table 1). The duration of implantation ranged from 141 to 1427 days. The explants were made available for pathological and material analyses after a legal examination in the laboratory of pathology and patients' consent was granted. The meshes were explanted together with the tissue capsules. In case of separation of the capsule from

the mesh, both of them were analyzed, separately. The explants were preserved in a 10% solution of formaldehyde.

Methods of the Analyses

A) Macroscopic Observations

The explants were first observed with naked-eyes and then photographed using a digital camera. The pictures were processed with Adobe Photoshop CS. The explants were measured for size and weight, with reference to their size and weight at implantation. The shrinkage was calculated as the ratio of the size of the explant over its size at implantation. The dimensions of the explants were measured by placing them on a grid paper (as shown in Table S1A). The grid paper has a minimum unit of 1 mm, allowing for the determination of the size, area, and other parameters of the explants by counting the grid units. The original area of the mesh at implantation was estimated by assuming the mesh was rectangular, with the maximum measured length and width of the explant taken as its original length and width.

B) Tissue Structure Characterizations

After the macroscopic observations, the explants were carefully dissected to examine their biointegration. A particular attention was paid to the stiffness of the explants, their encapsulation, and the fibrous tissue formation. At least two specimens per explant were selected for histology. In addition, two small coupons (0.5 cm × 0.5 cm) of the fabric from each explant and from a pristine mesh similar to that explant were cut for textile investigations.

- Light microscopy: Gradually dehydrated specimens were embedded in paraffin, cut into 5 µm slides with a microtome, and then stained with hematoxylin and eosin (HE) for general observations, Masson's trichrome for collagen, Verhoeff for elastin fibers, and red picrosirius to observe collagen bundles under a polarized microscope.
- Scanning electron microscopy: After post-fixation in osmium tetroxide, the specimens were rinsed in distilled water and dehydrated in ethanol solutions of increasing concentration until absolute ethanol, and then transferred to pure acetone. Final drying was achieved in hexamethyldisilazane. After gold-palladium coating, the specimens were observed with a scanning electron microscope SEM JSM-IT200 (Jeol, Tokyo, Japan) at accelerating voltages from 15 kV to 25 kV.
- Transmission electron microscopy: After post-fixation in osmium tetroxide followed by uranyl acetate staining, the dehydrated specimens were embedded in epoxy then sliced. Further to additional stains with lead citrate and uranyl acetate, the specimens were observed in a transmission electron microscope TEM-1230 (Jeol, Tokyo, Japan) at an 80 kV accelerating voltage.

C) Material Analyses

The explanted meshes were made of PP knits with or without ePTFE. The material analyses were performed on the different layers of the composite hernia meshes. The tissues

attached to the meshes were first removed according to the protocol established in our laboratory. The poorly attached tissues were removed with tweezers. Then, the specimens were boiled for 10 minutes in a 99.5% solution of cyclohexanone ($C_6H_{10}O$). After cooling down to room temperature and staying in the same solution overnight, the specimens were rinsed three times in distilled water and air dried. Each specimen was observed under a 10× magnification to confirm the complete removal of the tissues. If any trace of tissue was found, the procedure was repeated.

- Fabric structure and fabric count: The number of broken filaments in the knitting fabric or picks in ePTFE membrane were counted under a compound microscope set to 40× magnification (Nikon CH-2, Nikon Imaging (China) Sales, Shanghai, China). An MB-Ruler software was used to calculate the numbers within 1 mm. At least five locations on each specimen were counted and the data were averaged.
- Thickness: A thickness gauge (CH-12.7-BTSX, Shanghai Liuling Instrument, Shanghai, China) with 0.001 mm division was used to measure the fabric thickness after cleaning. The diameter of the gauge head was 5 mm, with an area of 19.63 mm^2. The testing pressure was 22 kPa ±5 kPa (44 g ±10 g). For each specimen, five randomly selected locations were tested and the data were averaged.
- Mass: It was measured with an electronic analytical balance (FA2004, Shanghai Liangping Instrument, Shanghai, China) to 0.1 mg resolution. Specimens of 1 cm × 1 cm were randomly sampled from three locations of the cleaned fabrics and weighed five times to calculate the average mass per unit area (g/cm2).
- Porosity (P): P is defined as the ratio of the area uncovered by filaments to the nominal area of the fabric. The total pixels of the picture of the fabric photographed at 20× magnification were determined, together with the total pixels of the pores in the picture that were selected by the Magic Wand Tool in Photoshop software. P was calculated as the ratio of the total pixels of the pores to the total pixels of the whole fabric.
- Number of filaments per yarn: Fabric yarns were randomly selected from ten different locations and split with tweezers under a magnifying glass. The number of the filaments in each yarn was counted. Special attention was paid to avoid yarn breakage and fiber entanglement.
- Stitch density: The number of stitches was determined by counting the number of wales along 5 cm of the width and the number of course along 5 cm of the length of the fabric. The wale density (wales/cm) and course density (courses/cm) were then calculated by dividing these counts by 5.
- Filament diameter: Ten filaments were randomly selected from 10 different locations from the cleaned fabrics. They were photographed with the compound microscope Nikon CH-2 fitted with a CCD camera at a 100× magnification. The filament diameter was measured with MB-Ruler software that was calibrated with a standard scale bar.

D) Chemical Analyses

Fourier Transform Infrared (FTIR):

The surface chemistry of the cleaned fabric specimens was examined with a Fourier transform infrared-Raman spectrophotometer (Nexus-670, Thermo Fisher Scientific, Waltham, MA, USA). The specimens were flattened and pressed against the crystal prism of the attenuated total internal reflectance (ATR) system to observe the absorption bands. The spectra were analyzed using a proprietary software (Omnic V 6.0).

Differential Scanning Calorimetry (DSC):

The thermal properties of the cleaned fabric specimens were measured with a Model 204F1 DSC (Netzsch Scientific Instruments (Shanghai), Shanghai, China). Specimens of approximately 3 - 4 mg were loaded into aluminum pans and sealed. The pans were heated from 50 °C to 300 °C at a programmed heating rate of 10 °C min^{-1}. Then the specimens were rapidly cooled to 50 °C and maintained at this temperature for 15 minutes before being heated again to 300 °C at the same heating rate. Data were collected and analyzed with the Proteus Thermal Analysis software to calculate the onset and peak temperatures, heat of fusion, crystallinity, and glass transition temperature (Tg) of all endotherms and exotherms.

RESULTS

Gross Observations

The thickness of the tissue encapsulated meshes was found highly variable (Fig. 1). The explants were thinner in case of monolayer fabric or membrane (Fig. 1A). The composite meshes involving both fabric and membrane were much thicker (Fig. 1D). We therefore classified the explants as follows, 1 layer PP, double-layer PP, double-layer PP with 3D structure, single ePTFE membrane, 1 layer PP + ePTFE membrane, and double-layer PP + ePTFE membrane (Table 1). More detailed information, including geometric structure data, about these 11 explants can be found in Table S6A-B in supplementary information.

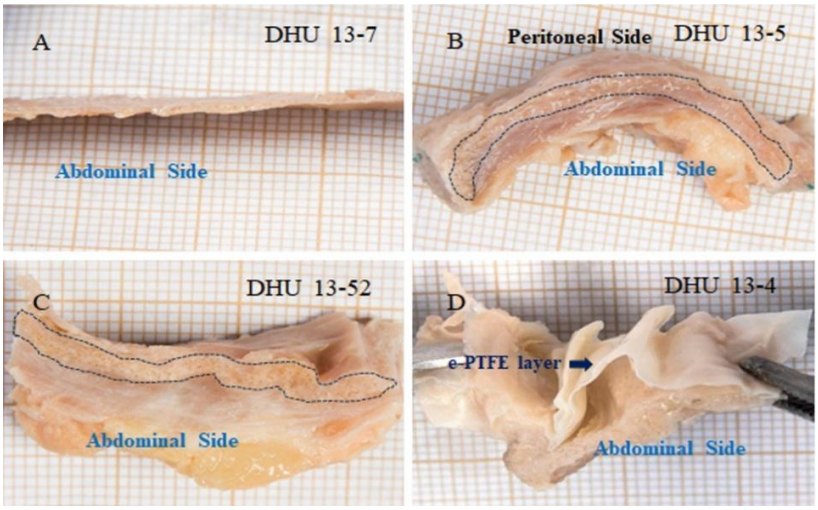

Figure 1: Tissue encapsulation of four clinically retrieved hernia meshes with four distinct structures. (A) A single-layer PP mesh; (B) A double-layer PP mesh; (C) A double-layer PP mesh with a three-dimensional structure; (D) A double-layer PP mesh combined with an ePTFE anti-adhesion barrier.

Table 1: Structural characteristics and clinical information of 11 mesh explants

Code	Construction of the devices	Cause of explanation	Duration (days)	Fixation	Symbol
DHU 13-3	single-layer PP	Recurrence	n/a	Sutures	
DHU 13-7		Recurrence	141	Sutures	
DHU 13-10		n/a	n/a	Sutures	
DHU 13-5	double-layer PP	Recurrence	1427	Sutures	
DHU 13-52	double-layer PP with 3D structure	Recurrence	n/a	Sutures	
DHU 13-11	Single ePTFE membrane	Recurrence	1035	Metallic clip	
DHU 13-13	single-layer PP + ePTFE membrane	Recurrence	958	Sutures	
DHU 13-2	double-layer PP + ePTFE membrane	Infection	1050	Sutures+ Metallic clip	
DHU 13-4		Recurrence	683	Sutures	
DHU 13-6		Recurrence	600	Sutures+ Metallic clip	
DHU 13-57		Infection and fistulae	n/a	Sutures+ Metallic clip	

The visceral side of the explants was smooth and glistening for most of the explanted meshes, likely without any fabric structure exposed to the intestine. Occasionally, the multi-layer meshes were irregularly folded in an accordion fashion, providing anchorage to tissue growth. The parietal side was irregular, incorporating various amounts of fatty tissues. The fabric structure was occasionally visible (Table S1A to S1F(B)). In the case of heavy accordion pleating of the ePTFE membrane, there were some tissues ingrowth in the invaginations of the structures (Table S1A, S1F(B)).

When looking at the change in size, all the meshes showed various levels of shrinkage (Fig. 2). The shrinkage of the single-layer PP meshes was much smaller than that of the double-layers PP meshes or the double-layers PP with 3D structure, although the weight of those meshes are similar. The shrinkage of DHU 13-3, DHU 13-5, and DHU 13-52 was 39.54%, 50.49% and 67.73%, respectively (Fig. 2A). Interestingly, the shrinkage of the single ePTFE membrane (DHU 13-11 at 49.75%) was much higher than ePTFE with single-layer PP mesh (DHU 13-13 at 20.73%). When an ePTFE membrane was used to repair the abdominal wall, tissues on the parietal side were irregularly and compactly attached with the ePTFE (Fig. 3C, Table S2D), causing shrinkage. By contrast, if there was a PP layer, tissues were found

uniformly grown inside the pores of the PP mesh and anchored to the ePTFE layer, thus decreasing the shrinkage of the mesh (Table S2E). The thickness of the ePTFE membrane was much thicker in the sole ePTFE mesh (DHU 13-11, 1.18 mm) than in the ePTFE + PP mesh (DHU 13-13, 0.21 mm) (Fig. 4). This might be another reason causing the difference in shrinkage.

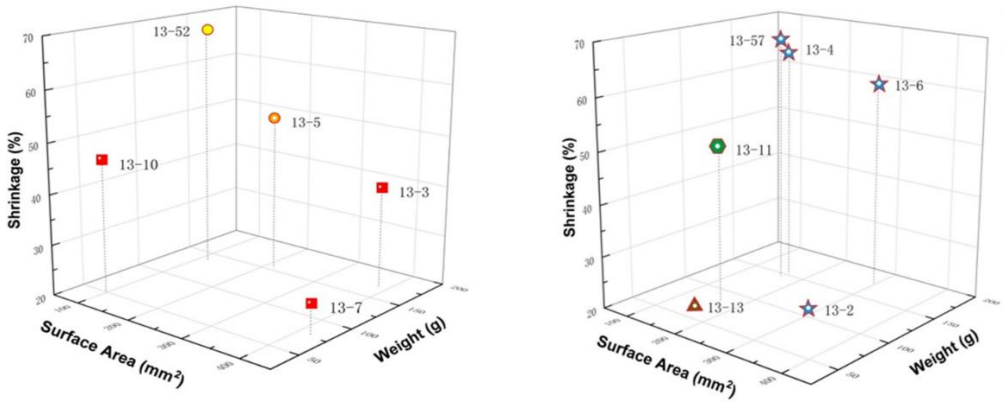

Figure 2: Impact of hernia mesh area and weight on shrinkage. (A) Single-layer and double-layer PP meshes; (B) A single ePTFE membrane mesh, a mesh of single-layer PP combined with an ePTFE anti-adhesion membrane, and four meshes of double-layer PP combined with an ePTFE anti-adhesion membrane.

Biointegration of the Meshes within the Abdominal Wall

The histology of the explants can be found in Fig. 3 and Table S2A to Table S2F(B). Overall, fibrous tissues covered every prosthesis. The mesh fabrics were encroached within straight and densely stretched bundles of collagen whose filaments did not demonstrate any waviness but featured a high density of scar tissue with various degrees of collagen aggregation. Different types of immune cells infiltrated the voids of the fabric, including leukocytes and monocyte, macrophages and giant cells.

The single-layer PP explant DHU 13-7 and DHU 13-10 are lightweight, thin, and are made of fine filaments and have about 35% porosity (Figs. 4, 5). They showed haemorrhages, fibrosis, and foci of necrosis (Table S2A, Table S3A(C)); but the lesions were less extensive compared with the double-layer PP mesh DHU 13-5 that is heavier and much thicker (Figs. 4, 5, Table S2B, Table S3B). The thickest PP mesh with 3D structure (DHU13-52) showed more important fibrosis and inflammation (Table S2C, Table S3C). The two infected explants (DHU 13-2 and DHU 13-57) showed quite different inflammation status. In DHU 13-2, most immune cells surrounded the PP fibers (Fig. 3A, 3B, Table S2F(A), Table S3F(A)), whereas in DHU 13-57, immune cells were primarily distributed inside the infected tissues, where a greater amount of PP fiber debris was also identified (Table S2F(B), Table S3F(D)). The 3D architecture of PP mesh was suspected to provide more void space for the infiltration of immune cells. The long-term inflammation caused thicker and denser hyperplastic scar tissues (Table S2C).

DHU 13-11 (single layer ePTFE) was the sole explant that illustrated the biological integration between abdominal wall and ePTFE membrane. The micropores in ePTFE permitted collagen infiltration (Fig. 3C, 3D, Table S2D, Table S3D). The collagen fibers at the interface of the ePTFE showed a tight and straight structure devoid of any waviness. In

comparison, the ePTFE membranes in other multilayer meshes were detached from the tissue encapsulated fabric (Fig. 3A, Table S2F(A,B)).

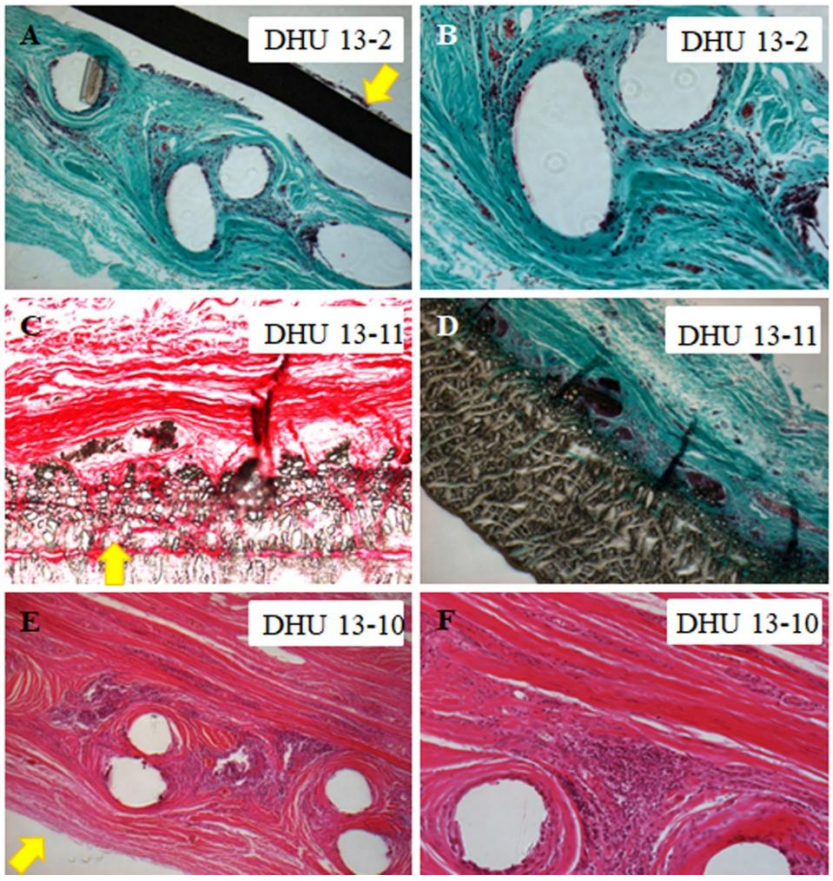

Figure 3: Histological images stained with Masson's trichrome (blue) and HE (pink), showing the integration of typical PP fibers and ePTFE membrane with fibrotic tissues, as well as the foreign body reaction around PP fibers. The arrows indicate the peritoneal side of the section. (A, B) Integration of PP fibers with surrounding tissues and the separation of the ePTFE anti-adhesion barrier; (C, D) Infiltration of tissues into the microfibrous ePTFE mesh; (E, F) Integration of PP fibers with surrounding tissues and the dense and thin fibrotic tissue.

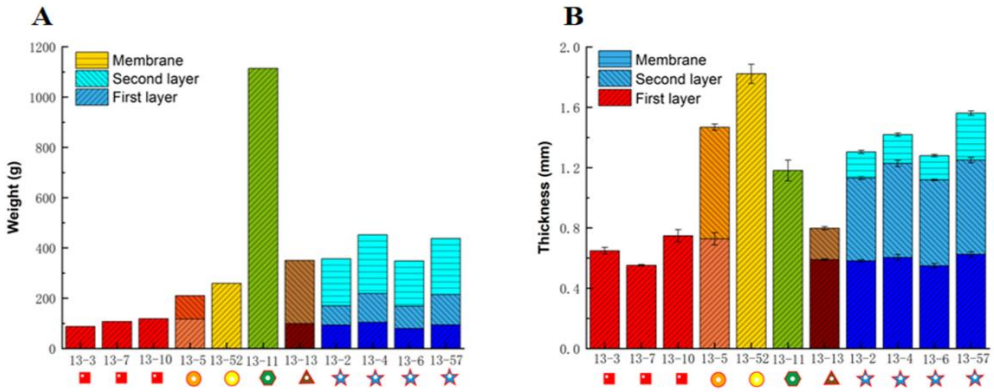

Figure 4: Comparison of the weight (A) and thickness (B) of the hernia meshes and their different layers.

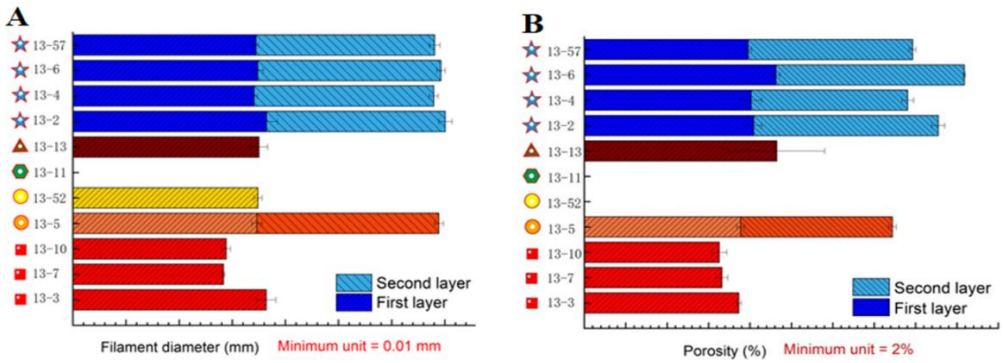

Figure 5: Comparison of fiber fineness (A) and porosity (B) of the explanted PP meshes and their different layers.

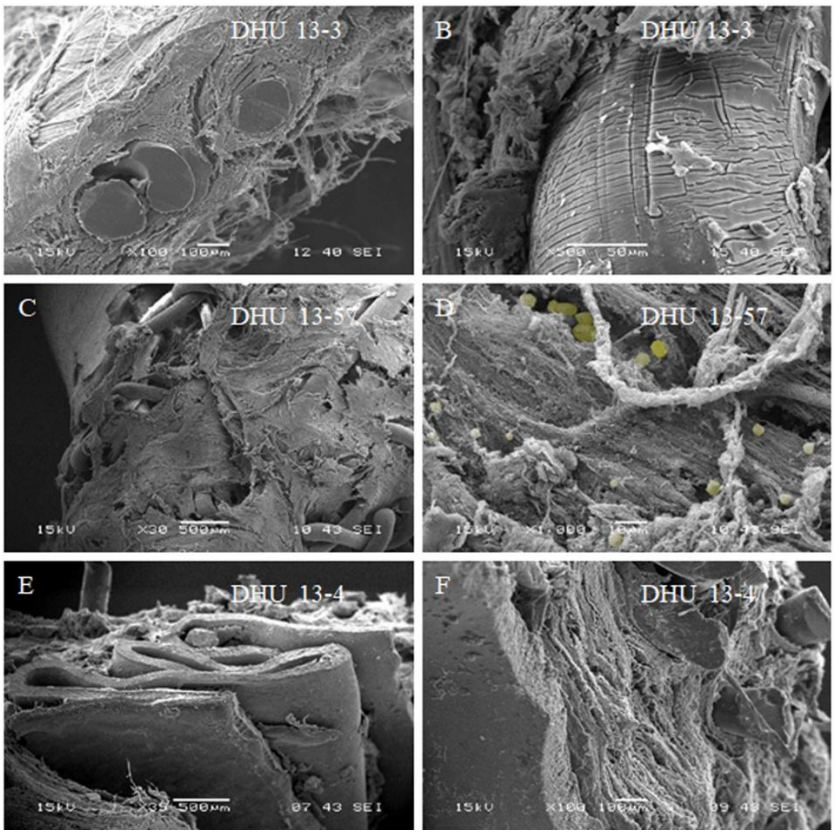

Figure 6: SEM revealed representative adverse reactions between implants and tissues. The PP fibers were tightly encapsulated within organized tissues (A), with surface corrosion and degradation occurred during prolonged implantation (B). Disorganized tissue encapsulation around multilayer mesh fibers (C) and Staphylococcus aureus concealed within tissue interstices (D) were noted. Wrinkling of the ePTFE anti-adhesion layer (E), attributed to the contraction of the fibrotic tissues that encapsulated the PP layer of this multi-layer hernia mesh (F).

The fibrosis tissues encapsulating the PP fibers showed no difference between the PP mesh and the PP/ePTFE mesh, with dense collagen fibers and immune cells surrounding the fibers (Fig. 3A, 3B, vs. 3E, 3F). Some PP debris were noticed in the fibrous capsule with haemorrhages and necrotized foci penetrated the ePTFE structure. The tissues and fibers of

the explants were observed with more details (Table S3A(A) to S3F(D)). Very dense and randomly oriented collagen fibers coved the prostheses compactly. Those tissue fibers showed almost no waviness, which means that the fibrosis tissues are stiff and compact. The PP fabric pattern can be clearly observed in some samples (Table S3A(B), arrows). Two typical factors affected the long-term biocompatibility of the implants. One is the foreign body reaction caused by the PP mesh, and the other is the damage caused by the inflammation to the PP fibers such as the cracks on the supposedly non-degradable PP materials (Fig. 6, Table S3A(A), Table S3E). Noticeably, the mesh made of double-layer PP and an ePTFE membrane was severely shrank (DHU 13-4), as the ePTFE membrane was folded in an accordion way (Table S3F(B), cross section).

Tables S4A to S4F(B) present the ultrastructure of the scar tissues in all explanted meshes observed under TEM. Generally, the collagen bundles were dense and compact. Some typical giant cells and macrophages were observed (Table S4A, Table S4F(A)). Some non-identified foreign body fragments and abnormal tissue structures appeared between the bundles of collagen (arrows, Table S4D, S4F(B)). An interesting phenomenon can be observed: the collagen bundles around the immune cell were relatively lose with fine diameters, and discontinuous. The TEM observations of the immune cells such as macrophages and foreign body giant cells suggest that these cells may have contributed to the regulation of the dynamic reconstruction of the collagen fibers (Fig. 7). The existing and state of the immune cells are the key factors determining the degree of mesh fibrous encapsulation.

The Textile Structure and the Chemical Component of the Mesh Determine the Repair Results

SEM images (Fig. 6, Table S5A) reveal that the three different single-layer PP meshes exhibited various degrees of cracking on the PP fibers, while the DHU 13-7, which adopted a lock-stitch weaving structure, showed the least degree. This is likely due to the fabric structure that matches well with the mechanical properties of the abdominal wall, leading to a better tissue integration and mechanical fatigue resistance without causing a strong foreign body reaction or oxidative erosion by the tissue. Therefore, constructing mechanically compatible fabric structures may help reduce stress anomalies and, in turn, minimize scar tissue formation (Table S5A). Compared to single-layer PP meshes, double-layer PP meshes such as DHU 13-5 showed more cracks and fragments, possibly because of the increased number of fibers and the structural complexity that lead to greater stress concentration and friction, triggering a stronger inflammatory response (Table S2B, Table S3B, Table S5B). In addition, it can be seen that the surface of DHU 13-11 (single-layer ePTFE film, Table S5D) has many micro-voids, providing points of attachment that facilitate scar tissue ingrowth, leading to tissue contraction. Thus, we suggest to pay more attention to the surface properties of the meshes, which may play a crucial role in the long-term effectiveness of the meshes. The more complex the fabric structure and the more layers it has, the easier it is to create an environment of abnormal stress, which is often the primary cause of long-term inflammation in the abdominal wall. Long-term inflammation further oxidizes the mesh materials, increasing the number of cracks and material fragments, forming a vicious circle that ultimately leads to recurrence of the hernia (Tables S5F(A) – S5F(B)). Selecting appropriate patch materials and their structures to integrate and remodel

the mechanical environment of the abdomen is critical for reducing complication and improving surgical success rate.

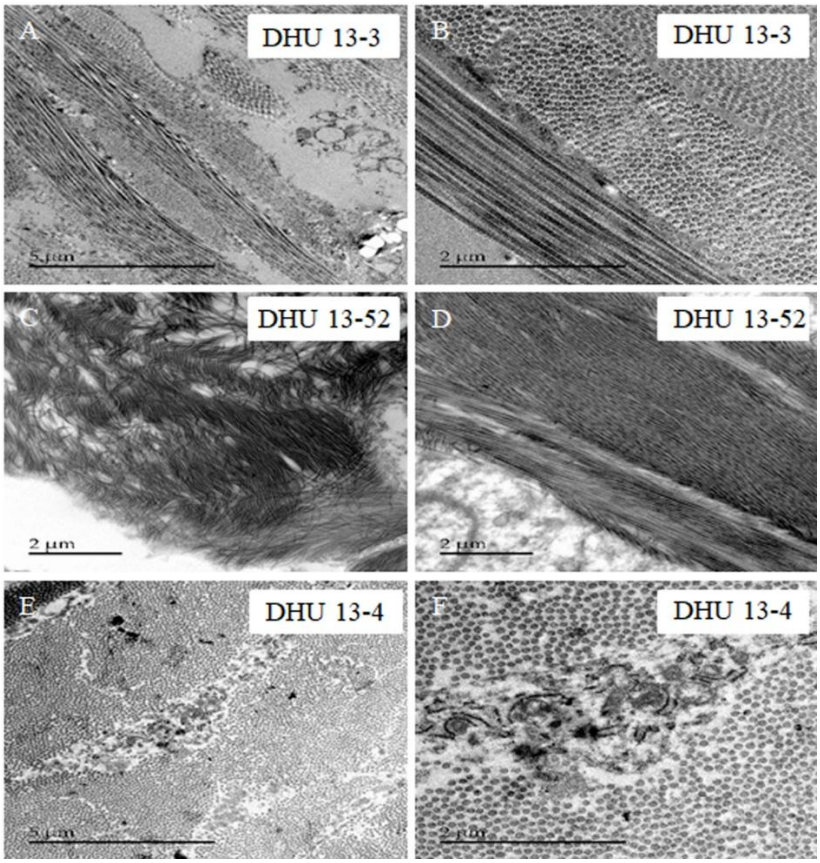

Figure 7: Typical TEM observations of the fibrous capsular tissue surrounding hernia mesh. (A,B) The collagen fibers in the tissue surrounding the single-layer PP mesh are relatively aligned and organized; (C, D) The collagen fibers in the tissue surrounding the multi-layer structured mesh are densely packed but disordered and oriented in multiple directions; (E) Infiltration of immune cells is still observed within the newly formed tissue; (F) is a magnified view of a specific region from image E.

Chemical Analyses

PP Surface Oxidation

Infrared spectroscopy can analyze chemical changes that occur in vivo in polymers. The FTIR spectra revealed differences in chemistry among the cleaned PP meshes with different fabric structures. For example, the hydroxyl (-OH) stretching near 3300 cm^{-1} of the single-layer PP mesh (DHU 13-7) is weaker than that of other single-layer PP meshes (DHU 13-3, DHU 13-10), indicating fewer hydroxyl groups generated in vivo by oxidation. The FTIR data are supported by SEM images that show negligible cracks on PP fibers (Table S7A). The hydroxyl stretching peak of the double-layer PP meshes is stronger than that of the single-layer ones, suggesting severer oxidations, consistent with the SEM results. For the double-layer PP + ePTFE composite mesh (DHU 13-4), the hydroxyl stretching vibration detected on PP fibers is even stronger, accompanied by severe cracks on the PP fiber surface and a

significant overall shrinkage of the fabric. The FTIR spectrum of the ePTFE layer changed little, an indication that ePTFE has stronger chemical stability in vivo (Table S7F(B)).

Change in PP Aggregation Structure

DSC is commonly used to analyze the thermal properties of polymer materials, with melting temperature being an important indicator of polymer aggregation structures. As shown by the DSC figures in Tables S7A-S7F(D), the melting temperatures of the single-layer PP meshes with different fabric structures vary. The melting temperature of DHU 13-7 is 171.63°C, which is higher than that of DHU 13-3 at 168.85 ° and DHU 10-10 at 170.06 °C. The melting temperature of PP tended to decrease as the degree of oxidation increased. The oxidation process led to chain scissions in PP molecules, forming shorter molecular chains with lower melting points. This result is consistent with the findings from infrared and SEM analyses. In composite meshes of PP and ePTFE, the melting temperature of PP further decreased. For instance, the melting temperature of PP in DHU 13-13 (single-layer PP fabric + ePTFE membrane) is 166.29 °C and the melting temperature of PP in DHU 132 (double-layer PP and ePTFE) drops to 165.33 °C and 166.22 °C, indicating that PP in composite meshes experienced severer oxidation in vivo, accompanied by intense foreign body reaction, issue contraction and mesh shrinkage rate. In conclusion, greater attention should be paid to the chemical stability and mechanical compatibility of meshes in vivo, which is significant for reducing inflammation, minimizing scar tissue formation, alleviating patient suffering, and reducing recurrence rate.

DISCUSSION

There is a plethora of commercially available hernia mesh products and the selection is not easy. But it is important to bear in mind that a hernia mesh is a medical implant specifically designed to treat patients.

The selection of a device for implantation is based upon mutual confidence between the surgeons and the manufacturers to better serve the patients. This series of investigations permits us to determine the strengths and the limitations of the hernia meshes and give manufacturers clues about the directions to undertake to better fulfill the patients' and surgeons' needs. The regulatory agencies represent a sound reference for the surgeons and the patients that devices commercially available such as the hernia prostheses improve the capacity to treat more abdominal wall hernia. This confidence is based upon continuous reassessment of the risks and benefits of the devices during the lifetime of the implant. As stated by the Clinical Device Group Inc., such an assessment is based upon [16, 20]:

- The data acquired by the manufacturers to become FDA approved or to obtain the CE mark, despite limited access to FDA reviews.
- The clinical investigations sponsored by the manufacturers.
- The scientific literature base upon bench studies and patient follow-up.
- The randomized clinical experience and possibly the results of analysis of explanted devices harvested during retrieval programs.

Should adverse events occur, it is mandatory to discriminate between device-related and patient-related. These should be disclosed to the patients. Since 1984, the FDA Material Device Reporting (MDR) regulations have required manufacturers to notify the FDA of severe adverse events and/or deaths associated with medical devices. Considerable efforts were deployed since 1990 to device tracking after their clearance to market. In Canada, Canadian Medical Devices Sentinel Network (CMDSNet) encourages the reporting of medical device problems by medical device users together with manufacturers. In MHRA, the UK, there is an obligation for the manufacturers to report adverse events to the users (healthcare suppliers and patients). The same rule is now applied in China. In-depth investigations of explanted devices have considerably changed the practice of surgery over the last few decades. Therefore, any incidence either patient-related or device-related must be reported because detailed analyses will help to improve the quality of the hernia meshes, to better focus on clinical indications, and to keep hernia prostheses classified as nonhazardous.

The manufacturers' decision to commercialize an implant is to provide the surgeons and the patient with a device that will fulfill the 3Bs rules and guarantees a lifelong service without device-related adverse events [32]. Let us summarize them as follows:

- Biofunctionality: The device should be easy to deploy at the precise site decided by the surgeon to properly reinforce the abdominal wall and be anchored safely.
- Biodurability: The device should be durable and never stretch, or shrink, during its in vivo lifetime. More specifically, the prostheses shall be both chemically and physically stable, even in biologically hostile environment.
- Biocompatibility: This means the biointegration of the prosthesis to regenerate a wall structure that mimics a healthy abdominal wall. The foreign materials shall be considered as scaffold to regenerate the abdominal wall. The reorganization of collagen is of specific importance and ideally the collagen bundles must show waviness to guarantee the softness of the reconstruction.

Under these circumstances, a retrieval program of explanted devices represents a sound contribution to the continuous assessment of medical devices. The myriads of devices commercially available for hernia surgery is a crystal clear indication that there is still no flag in the field despite considerable effects of clarification.

The implantation of meshes to reinforce the abdominal wall is said to cause fewer recurrences and less postoperative pain with respect to tension-based repair. Further to Usher in 1959 [12] and Lichtenstein in 1989 [5], mesh repair is acknowledged as the most reliable approach. Unfortunately, adverse events are not uncommon [33-35]. The plethora of devices commercially available and the poor understanding of vocabulary between surgeons, manufacturers and engineers lead to Kafkaesque situations. Despite remarkable efforts by pioneers like Klinge [3] and Deeken [29] who pioneered the development of sound classifications over the last decade, the vocabulary is still at odds between the partners. The surgeons understand lightweight, pore size, polypropylene and resorbable. In the meantime, the engineers talk about tensile strength, suture pull out strength, stitch density, lapping diagram and chain notation. Under these circumstances, the analysis of explanted devices oblige engineers and surgeons to open the doors to a better understanding of the phenomena. More practically, the recurrence of the hernias shall be explained. What are

the observations carried out on the explants that are the most striking: the shrinkage of the mesh reached very high percentages and the biostability of the polymers must be paid attention. Let us address these issues serially.

The tissue ingrowth through the mesh structure leads compact and well collagenized tissues from moderately cellular to acellular. There is almost no vascularisation as the fibrous tissue is highly compact. Inflammatory cells and macrophages were present at the contact with the foreign material and became more intensive in the situations of mesh degradation, either chemical degradation or mechanical degradation. The scar tissue infiltrates any open structure, either knitted PP or ePTFE.

Tissue encapsulation can be considered as a hypertrophic scar formation similar to wound healing of deep and extensive burns. The new collagen is made of thick bundles or parallel fibrils without wavy structure. In addition, the poor blood supply may induce nutrient deprivation, and thus explains the presence of necrosis.

The second issue is the durability of the device. The ingrowth of the fibrous tissue into the pores of the expanded PTFE stretched the fine polymer fibrils that hold the polymer nodes, and eventually ruptured the ePTFE structure. The degradation of the PP is more a surface phenomenon caused by the surface oxidation. As long as the chemical degradation does not go deep, the PP fiber strength is only marginally reduced. However, the inflammatory reaction might be continuously exacerbated. The polymers must therefore be selected more cautiously with traceability of the source. In addition, PP fibers are very sensitive to mechanical damage. Regarding the PP, one should be aware about its fragility during handling, more specifically its sensitivity to needle holders. In addition, gamma sterilization must be prohibited because it causes the destruction of the PP polymer chains.

Compared to PP, the PVDF shows similar strength with higher extension at break. It has less delayed extension when under tensile creep testing [36]. The resistance to surgical trauma caused by needle holders compares favourably to PP. In addition, PVDF can be sterilized by ß or γ irradiation and so can avoid ethylene oxide and chlorofluorohydrocarbon, which makes PVDF more ecologically acceptable [37]. The greater extensibility might require the surgeon to slightly modify its technique but it would probably be a major advantage in vivo to keep the reconstruction much softer. In addition, the PVDF holds piezoelectric characteristics and the potential benefits for the biocompatibility must be investigated [38]. The piezoelectricity is the ability of the materials to polarize and display charges on surface by stress and/or strain. For biomedical application, piezoelectric materials allow the delivery of electrical stimulus without the need of a power source. The piezoelectricity of single collagen fibrils has been studied using piezoforce microscopy-PFM, showing lateral piezoresponse at the fibril axis and a negligible vertical and radio piezoresponse, revealing the unidirectional polarization along the fibril collagen axis [39].

Implantation of PVDF meshes in sheep for up to 24 months, when compared to PP meshes, demonstrated superior morphological and chemical stability by showing no sign of any change in either surface chemistry or fiber surface morphology [40]. PVDF meshes infected with *Staphylococcus (S.) aureus* and then implanted in rats for up to 21 days also showed less intensive inflammatory reactions compared with similarly infected PP meshes [41]. Furthermore, in a sex and age-matched clinical trial, PVDF meshes were compared with ePTFE meshes in the treatment of incisional hernia, showing similar performance in terms of operation time, hospital stay and recurrence rate [42].

While we would like to consider the hernia meshes as a scaffold to support tissue regeneration and biointegration, we must be aware that patients treated for hernia repair show connective tissue alteration in their abdominal wall. These alterations include connective tissues at locations distant from hernia sites as well. Abdominal wall hernias, like abdominal aortic aneurysms, are manifestations of a connective tissue disorder [41, 42]. Future investigation may elucidate obscure aspects of hernia pathophysiology and create novel targets for pharmaceutical and gene strategies for disease prevention and treatment. As hernia surgery is consistently on the rise, it is anticipated that the medical industry will continue to innovate and develop new generation of devices that will better fulfill patients' requirements.

In the meantime, the approval of the devices by regulatory agencies is critical. The introduction of new technologies represents a considerable challenge for the patients, the surgeons and the manufacturers. The ethics in introducing new surgical technology must be paid attention. The relationship between the patient and the surgeon is of paramount.

CONCLUSION

The hernia meshes contribute to the formation of scar tissues, incorporating stretched collagen fibers without any waviness. Continuous efforts must be paid to determine the most appropriate constructions and the best materials to serve as scaffolds for the development of soft and elastic scar tissue that incorporates wavy collagen fibers.

This comprehensive analysis of eleven hernia mesh explants, retrieved after up to four years of implantation, provides critical insights into the long-term host response and failure mechanisms of PP- and ePTFE-based prostheses. The central finding is the universal and significant shrinkage (12% to 53%) of all devices, driven primarily by the contraction of dense, fibrotic scar tissue that extensively encapsulates and penetrates the implant structures. A key pathological finding is the formation of straight, non-wavy collagen bundles within the encapsulating tissue, resulting in a stiff, non-compliant scar that lacks the elasticity of native abdominal wall. Material composition critically influences the host response. PP mesh promotes tissue ingrowth but undergoes surface oxidation and fragmentation, fueling chronic inflammation. ePTFE is chemically stable but often becomes poorly integrated, merely encapsulated, and prone to detachment in composite meshes. Furthermore, increased structural complexity (e.g., multi-layer, 3D designs) exacerbates the inflammatory response and material stress. Continuous efforts must be paid to determine the most appropriate constructions and the best materials to serve as scaffolds that prompt the development of a soft and elastic scar tissue incorporating wavy collagen fibers. Future designs should prioritize the regeneration of functional, wavy collagen to restore tissue elasticity and compliance. This requires a concerted focus on three principles: Biofunctionality (secure integration), Biodurability (long-term stability), and true Biocompatibility (minimizing chronic inflammation).

ACKNOWLEDGEMENTS

This work was supported in part by the Fonds de recherche du Québec (FRQ) though the research grant for the CHU de Québec - Université Laval Research Center (Reference: 30641), the Fundamental Research Funds for the Central Universities (Donghua University

NS2013), the National Nature Science Foundation (31100682 and 30972942), the 111 project "Biomedical Textile Materials Science and Technology" (B07024), the Engineering Research Center of Technical Textile Ministry of Education and the Science and Technology Commission of Shanghai Municipality (11DZ2292900).

REFERENCES

1. Miao, L., Wang, F., Wang, L. et al. Physical characteristics of medical textile prostheses designed for hernia repair: a comprehensive analysis of select commercial devices. Materials 2015;8:8148-8168. doi: 10.3390/ma8125453
2. Holzheimer, R.G., Hakim, N. The pathogenesis of mesh-induced inflammatory response and pain: Rationale for development of new mesh. Int J Biomed Clin Anal 2023;3:109-119. doi.org/10.61797/ijbca.v3i2.272
3. Zhu, L-M., Schuster, P., Klinge, U. Mesh implants: An overview of crucial mesh parameters. World J Gastrointest Surg 2015;7:226-236. doi: 10.4240/wjgs.v7.i10.226.
4. Read, R.C. Milestones in the history of hernia surgery: prosthetic repair. Hernia 2004;8:8-14. doi: 10.1007/s10029-003-0169-2.
5. Lichtenstein, I.L., Shulman, A.G., Amid, P.K., Montllor, M.M. The tension-free hernioplasty. Am J. Surg. 1989;15:188-193. doi: 10.1016/0002-9610(89)90526-6.
6. Weyhe, D., Belyaev, O., Müller, C., et al. Improving outcomes in hernia repair by the use of light meshes: a comparison of different implant constructions based on a critical appraisal of the literature. World J Surg. 2007;31:234-244. doi: 10.1007/s00268-006-0123-4.
7. Bellows, C.F., Smith, A., Malsbury, J., Helton, W.S. Repair in incitional hernias with biological prosthesis: a systematic review of current evidence. Am J Surg 2013;205:85-101. doi: 10.1016/j.amjsurg.2012.02.019.
8. Earle, D.B., Mark, L.A. Prosthetic material in inguinal hernia repair: How do I choose? Surg. Clin. N. Am. 2008;88:179-201. doi: 10.1016/j.suc.2007.11.002.
9. Bilsel, Y., Abcj, I. The search for ideal hernia repair, mesh materials and types. Int. J. Surg. 2012;10:317-321. doi: 10.1016/j.ijsu.2012.05.002.
10. Holzheimer RG. A Narrative review on polypropylene mesh complications in inguinal hernia repair - is titanized mesh an option? J Surg 2022; 7: 1549. doi.org/10.29011/2575-9760.001549
11. Abbas AW, Abo-Elsoad MF, Hindawi MD, Zeid MA, Kalmoush AE, Aboelkier MM, Aldemerdash MA, Mohamed RG, Elghadban H. Prophylactic mesh reinforcement in elective abdominal surgeries: a systematic review, meta-analysis, and GRADE evidence assessment. Hernia. 2025 Jul 11;29(1):230. doi: 10.1007/s10029-025-03421-9.
12. Usher, F., Gannon, J. Marlex mesh, a new plastic mesh for replacing tissue defects. J. Occup. Environ. Med. 1959;78:138-145. doi: 10.1001/archsurg.1959.04320010140023.
13. Antoniadi E, Ferreira NM, Vaz MF, Parente M, Ferraz MP, Silva E. Innovative strategies in hernia mesh design: Materials, mechanics, and modeling. Materials (Basel). 2025 Jul 26;18(15):3509. doi: 10.3390/ma18153509.
14. Meng C, Wei Q, Sun L, Zhang X, Liu Y, Gao J, Wei P, Yang Z, Yao H, Zhang Z. Effects of different mesh materials on complications after prophylactic placement for stoma formation: a systematic review and network meta-analysis. Hernia. 2024 Aug;28(4):1039-1052. doi: 10.1007/s10029-024-03068-y.

15. Levy, A.H., Wren, R.S., Friedman, M.N. Complications and recurrences flowing inguinal hernia repair. Ann. Surg. 1951;133:533-539.

16. O'Conner, A.B. The need for improved access to FDA review. J. Am. Med. Assoc. 2009;302:191-193.

17. Isenberg EE, Fry BT, Sinamo J, Howard RA, Ehlers AP, Shao JM, Jean RA, Telem DA. Long-term recurrence and the safety of mesh use after emergency ventral hernia repair. JAMA Netw Open. 2025 Nov 3;8(11):e2544303. doi: 10.1001/jamanetworkopen.2025.44303.

18. Klinge, U., Klosterhalfen, B. Modified classification of surgical meshes for hernia repair base on the analyses of 1,000 explanted meshes. Hernia, 2012;16:251-258. doi: 10.1007/s10029-012-0913-6.

19. Iakovlev, V.V., Guelcher, S.A., Bendavid, R. Degradation of polypropylene in vivo: A microscopic analysis of meshes explanted from patients. J. Biomed. Mater. Res. B. 2015. doi: 10.1002/jbm.b.33502.

20. US Food and Drug Administration. Reporting Adverse events. www.fda.gov/medicaldevices/deviceregulationandguidance/postmarketrequireements/reportingadverseevents/default.htm.

21. ECRI Institute releases top 10 health technology hazard reports for 2013. www.ecri.org/2014hazards. Consulted on 2014-01-09.

22. Surgical mesh for hernia repair. FDA Activities: https://fda.gov/medical devices/surgical-mesh-used-hernia-repair/surgical-mesh-hernia-repair/surgical-mesh-hernia-repair-FDA-activities. Consulted on April 22, 2025.

23. Coda, A., Lamberti, R., Martorana, S. Classification of prosthetics used in hernia repair based on weight and biomaterial. Hernia 2012;16:9-20. doi: 10.1007/s10029-011-0868-z.

24. Stabilini, C., Theodorou, A., Pawlak, M., Antoniou, S., Berrevoet, F., Bougard, H., Bracale, U., Capoccia Giovannini,.S., Fortelny, R., Gaarder, C., Garcia-Urena, M.A., Gilmore, K., Gomez-Ochoa, S.A., Köckerling, F., Mäkäräinen, E., Morales-Conde, S., Pecchini, F., Pereira Rodríguez, J.A., Quiroga-Centeno, A.C., Renard, Y., Romain, B., Schembari, E., Deerenberg, E. EHS guidelines on the management of primary ventral and incisional hernias under emergency conditions. J. Abdom. Wall Surg. 2026;5:16228. doi: 10.3389/jaws.2026.16228.

25. Zamkowski, M., Tomaszewska, A., Lubowiecka, I., Karbowski, K., Putko, M., Śmietański, M. Mechanical stability of new-generation meshes for M3 inguinal hernia repair: experimental pressure chamber testing of SWING-Mesh and 3DMax MID Anatomical Mesh. Wideochir Inne Tech Maloinwazyjne. 2025;20:409-414. doi: 10.20452/wiitm.2025.17990.

26. Maurer, M., Röhrnbauer, B., Feola, A et al. Mechanical biocompatibility of prosthetic meshes: A comprehensive protocol for mechanical characterization. J. Mech. Behav. Biomed. Mater. 2014;40:42-58. doi: 10.1016/j.jmbbm.2014.08.005.

27. Deeken, C.R., Thompson, D.M., Castile, R.M., Lake, S.P. Biaxial analysis of synthetic scaffolds for hernia repair demonstrates variability in mechanical anisotropy, non-linearity and hysteresis. J. Mech. Behav. Biomed. Mater. 2014;38:6-16. doi: 10.1016/j.jmbbm.2014.06.001.

28. Klinge, U., Klosterhalfen, B., Müller, M., et al. Shrinking of polypropylene mesh in vivo: an experimental study in dogs. Eur J. Surg. 1998;164:965-969. doi: 10.1080/110241598750005156.

29. Deeken, C.R., Abdo, M.S., Frisella, M.M., Matthews, B.D. Physiomechanical evaluation of polypropylene, polyester and polytetrafluoroethylene meshes in inguinal hernia repair. J. Am. Coll. Srg. 2011; 212:68-79. doi: 10.1016/j.jamcollsurg.2010.09.012.

30. Cobb, W.S., Peindl, R.M., Zerey, M., et al. Mesh terminology 101. Hernia 2009;13:1-6. doi: 10.1007/s10029-008-0428-3.

31. Mühl, T., Binnebösel, M., Klinge, U., Goedderz, T. New objective measurement to characterized the porosity of textile implants. J. Biomed. Mater. B Appli. Biomater. 2008;84:176-183. doi: 10.1002/jbm.b.30859.

32. Guidoin, R., Wang, L., Zhang, Z. Serving the good of the patient in cardiovascular implantology: The 3Bs' concept shall be heralded as the way to go. In Cardiovascular Explants: Biofunctionality, Biodurability and Biocompatibility. Eds. Robert Guidoin, Lu Wang, Ze Zhang. Springer 2025. pp. 1-12. https://link.springer.com/book/10.1007/978-3-031-85504-7

33. Kowalik, C.R., Zwolsman, S.E., Malekzadeh, A., Roumen, R.M.H., Zwaans, W.A.R., Roovers, J.W.P.R. Are polypropylene mesh implants associated with systemic autoimmune inflammatory syndromes? A systematic review. Hernia. 2022;26:401-410. doi: 10.1007/s10029-021-02553-y.

34. Fadaee, N., Huynh, D., Khanmohammed, Z., Mazer, L., Capati, I., Towfigh, S. Patients with systemic reaction to their hernia mesh: An introduction to mesh implant illness. J. Abdom. Wall Surg. 2023;2:10983. doi: 10.3389/jaws.2023.10983

35. Pizza, F., Iuppa, A., Maida, P., Pilone, V., Crucitti, A., Carmen, T.P.M., Morini, L., Marin, J.N., Petitti, T., Bertoglio, C., Marte, G., Sordelli, I., Gili, S., Lucido, F.S., Busciano, L., D'Antonio, D., Docimo, L., Gambardella, C. Postoperative outcomes and wound events in incisional hernia repair using hybrid mesh: results from a prospective multicenter italian study. Hernia. 2025;29:94. doi: 10.1007/s10029-025-03285-z.

36. Hong, T., King, M.W., Michielsen, S., Cheung, L.W., Mary, C., Guzman, R., Guidoin, R. Development of in vitro performance tests and evaluation of nonabsorbable monofilament sutures for cardiovascular surgery. ASAIO J. 1998;44:776-85. doi: 10.1097/00002480-199811000-00004.

37. Urban, E., King, M.W., Guidoin, R., Laroche, G., Marois, Y., Martin, L., Cardou, A., Douville, Y. Why make monofilament sutures out of polyvinylidene fluoride? ASAIO J. 1994;40:145-56. https://pubmed.ncbi.nlm.nih.gov/8003751/

38. Andrey, V., Koshevaya, E., Mstislav, M., Parfait, K. Piezoelectric PVDF and its copolymers in biomedicine: innovations and applications. Biomater. Sci. 2024;12:5164-5185. doi: 10.1039/d4bm00904e.

39. Bazaid, A., Zhang, F., Zhang, Q., Neumayer, S., Denning, D., Habelitz, S., Marina Ferreira, A., Rodriguez, B.J. Electromechanical coupling in collagen measured under increasing relative humidity. Materials (Basel). 2023;16:6034. doi: 10.3390/ma16176034.

40. Wang, H., Klosterhalfen, B., Müllen, A., Otto, T., Dievernich, A., Jockenhövel, S. Degradation resistance of PVDF mesh in vivo in comparison to PP mesh. J. Mech. Behav. Biomed. Mater. 2021;119:104490. Erratum in: J Mech Behav Biomed Mater. 2023 May;141:105786. doi: 10.1016/j.jmbbm.2021.104490.

41. Schmitz, S.M., Helmedag, M.J., Kroh, A., Heise, D., Klinge, U., Lambertz, A., Hornef, M.W., Neumann, U.P., Eickhoff, R.M. Choice of polymer, but not mesh structure variation, reduces the risk of bacterial infection with staphylococcus aureus in vivo. Biomedicines 2023; 11: 2083. doi: 10.3390/biomedicines11072083.

42. Verbo, A., Pafundi, P., Manno, A., Baccaro, R., Veneziani, A., Colli, R., Coco, C. Polyvinylidene fluoride mesh (PVDF, DynaMesh®-IPOM) in the laparoscopic treatment of incisional hernia: A prospective comparative trial versus Gore® ePTFE DUALMESH® Plus. Surg. Technol. Int. 2016;28:147-51. https://pubmed.ncbi.nlm.nih.gov/27042788/

43. Antoniou, G.A., Georgiadis, G.S., Antoniou, S.A., Granderath, F.A., Giannoukas, A.D., Lazarides, M.K. Abdominal aortic aneurysm and abdominal wall hernia as manifestations of a connective tissue disorder. J. Vasc. Surg. 2011;54:1175-81. doi: 10.1016/j.jvs.2011.02.065.

44. 44. Pūkas, A., Stankutė, D., Gudaitytė, J. Anaesthetic management of a patient with Marfan syndrome undergoing elective ventral hernia repair. Healthcare (Basel). 2025;14:34. DOI: 10.3390/healthcare14010034

Table 1: Structural characteristics and clinical information of 11 mesh explants

Code	Construction of the devices	Cause of the explanation	Duration (days)	Fixation	Mark
DHU 13-3	single-layer PP	Recurrence	/	Sutures	
DHU 13-7		Recurrence	141	Sutures	
DHU 13-10		/	/	Sutures	
DHU 13-5	double-layer PP	Recurrence	1427	Sutures	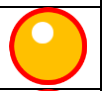
DHU 13-52	double-layer PP with 3D structure	Recurrence	/	Sutures	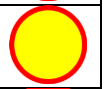
DHU 13-11	Single ePTFE membrane	Recurrence	1035	Metallic clip	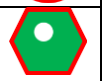
DHU 13-13	single-layer PP +ePTFE membrane	Recurrence	958	Sutures	
DHU 13-2	double-layer PP +ePTFE membrane	Infection	1050	Sutures+ Metallic clip	
DHU 13-4		Recurrence	683	Sutures	
DHU 13-6		Recurrence	600	Sutures+ Metallic clip	
DHU 13-57		Infection and fistulae	/	Sutures+ Metallic clip	

Table S1A: Observation of the explanted devices: One layer of PP mesh

Code	Explants		Implant size (cm)	Explant size (cm)	Shrinkage in each direction (%)	Implant surface (cm^2)	Explant surface (cm^2)	Shrinkage (%)	Explant weight (g)
	Parietal side	Visceral side							
DHU13-3	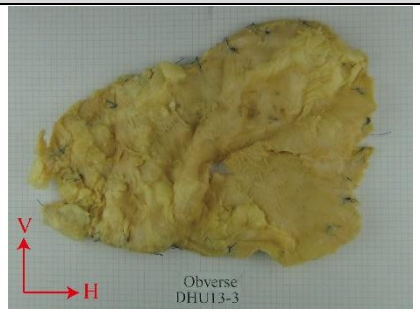	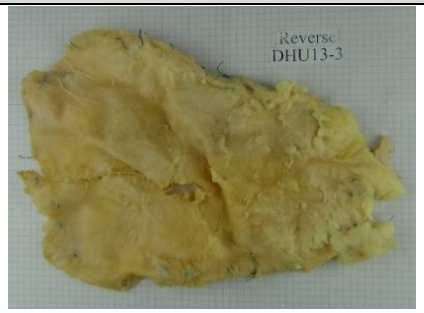	H: 32.00*	H: 26.00	H: 42.22	640.00*	386.92	39.54	167.86
			V: 20.00*	V: 18.00	V: 21.74				
DHU13-7 (141 days)	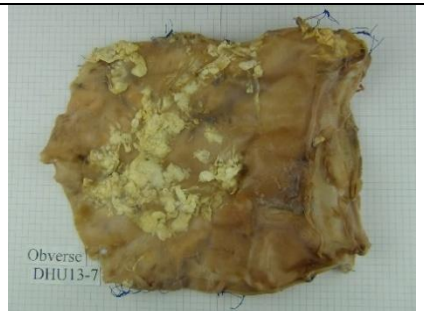	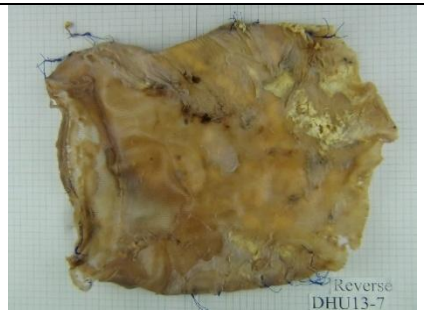	H: 30.50	H: 22.00	H: 27.87	619.16	422.41	25.38	76.37
			V: 20.30	V: 21.00	V: 0				
DHU13-10	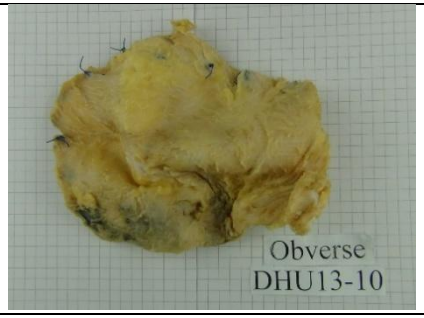	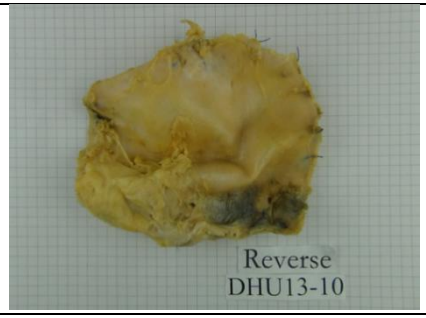	H: 14.00*	H: 13.00	H: 7.40	182.00*	98.81	45.60	49.45
			V: 13.00*	V: 10.00	V: 20.00				

Table S1B: Observation of the explanted devices: Two layers of PP mesh

Code	Explants		Implant size (cm)	Explant size (cm)	Shrinkage in each direction (%)	Implant surface (cm^2)	Explant surface (cm^2)	Shrinkage (%)	Explant weight (g)
	Parietal side	Visceral side							
DHU13-5 (1427 days)	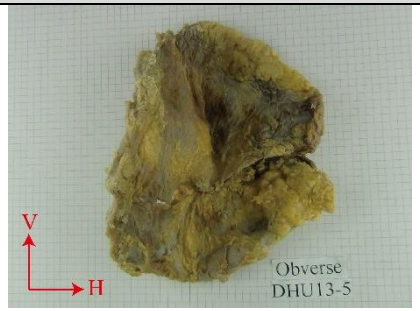	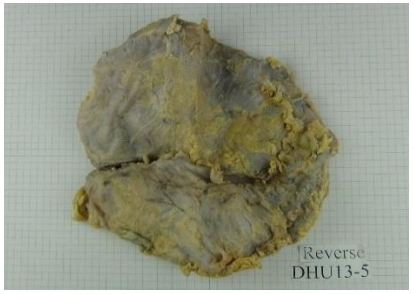	H: 23.50*	H: 19.00	H: 19.14	433.51*	214.62	50.49	154.44
			V: 23.50*	V: 17.50	V: 25.53				

Table S1C: Observation of the explanted devices: double-layer PP with 3-dimensional structure

Code	Explants		Implant size (cm)	Explant size (cm)	Shrinkage in each direction (%)	Implant surface (cm^2)	Explant surface (cm^2)	Shrinkage (%)	Explant weight (g)
	Parietal side	Visceral side							
DHU 13-52	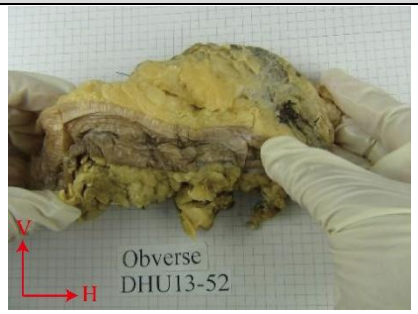	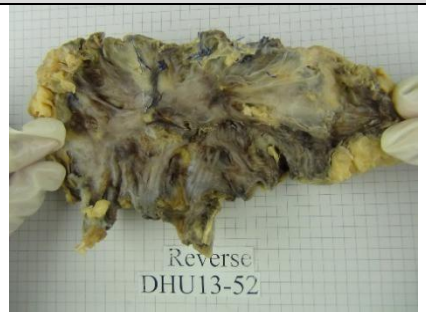	H: 22.00*	H: 19.50	H: 15.55	352.00*	113.57	67.73	138.00
			V: 16.00*	V: 13.00	V: 28.57				

Table S1D: Observation of the explanted devices: Single ePTFE membrane

Code	Explants		Implant size (cm)	Explant size (cm)	Shrinkage in each direction (%)	Implant surface (cm^2)	Explant surface (cm^2)	Shrinkage (%)	Explant weight (g)
	Parietal side	Visceral side							
DHU13-11 (1035 days)	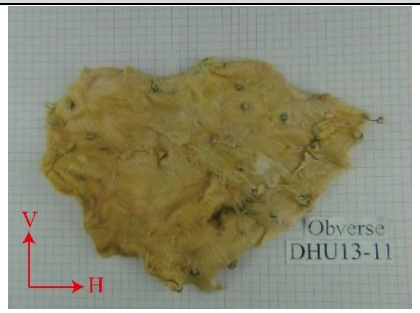	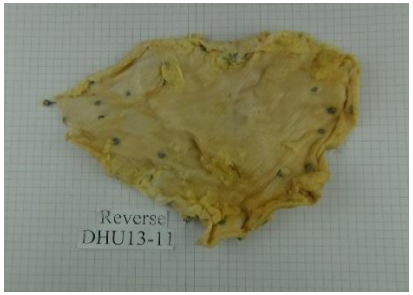	H: 22.00*	H: 19.50	H: 11.36	330.00*	165.83	49.75	82.42
			V: 15.00*	V: 13.00	V: 13.33				

Table S1E: Observation of the explanted devices: One layer of PP mesh + ePTFE membrane

Code	Explants		Implant size (cm)	Explant size (cm)	Shrinkage in each direction (%)	Implant surface (cm^2)	Explant surface (cm^2)	Shrinkage (%)	Explant weight (g)
	Parietal side	Visceral side							
DHU13-13 (558 days)		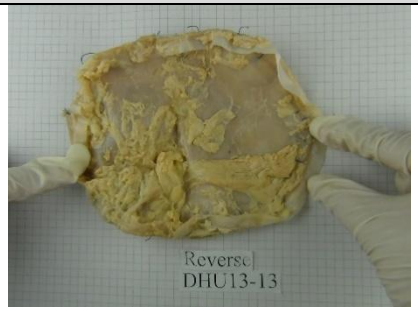	H: 18.00	H: 16.00	H: 11.11	197.82	156.81	20.73	58.12
			V: 14.00	V: 12.00	V:14.29				

Table S1F(A): Observation of the explanted devices: Two layers of PP mesh + ePTFE

Code	Explants		Implant size (cm)	Explant size (cm)	Shrinkage in each direction (%)	Implant surface (cm^2)	Explant surface (cm^2)	Shrinkage (%)	Explant weight (g)
	Parietal side	Visceral side							
DHU13-2 (1050 days)	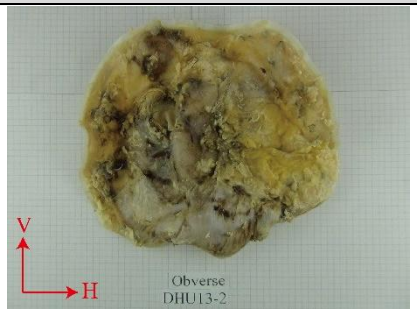	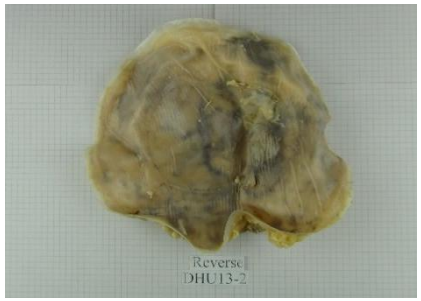	H: 24.60	H: 22.00	H: 10.57	378.50	299.05	20.98	102.36
			V: 19.60	V: 19.00	V: 3.06				
DHU13-4	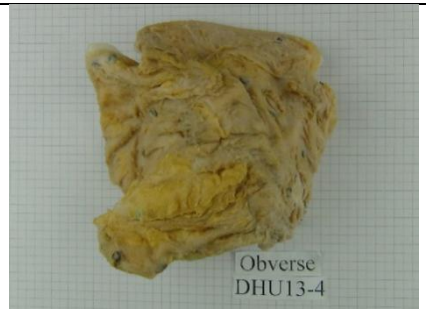	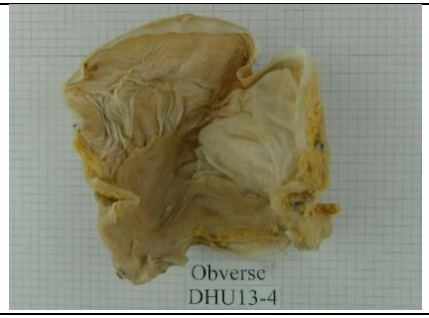	H: 25.00	H: 18.00	H: 28.00	500.00	162.29	67.54	145.66
			V: 20.00	V: 13.00	V: 35.00				

Table S1F(B): Observation of the explanted devices: Two layers of PP mesh + ePTFE membrane

Code	Explants		Implant size (cm)	Explant size (cm)	Shrinkage in each direction (%)	Implant surface (cm^2)	Explant surface (cm^2)	Shrinkage (%)	Explant weight (g)
	Parietal side	Visceral side							
DHU13-6	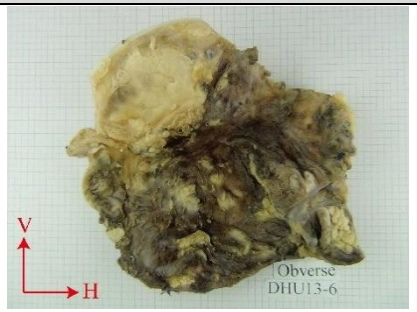		H: 32.50*	H: 24.00	H: 26.15	731.25*	294.66	59.70	177.18
			V: 22.50*	V: 18.00	V: 20.00				
DHU13-57	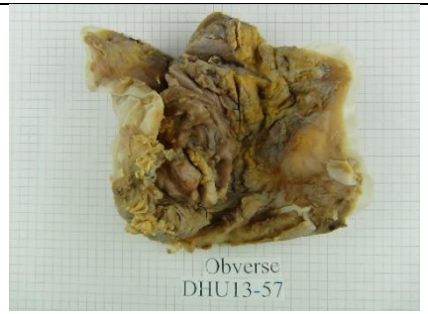	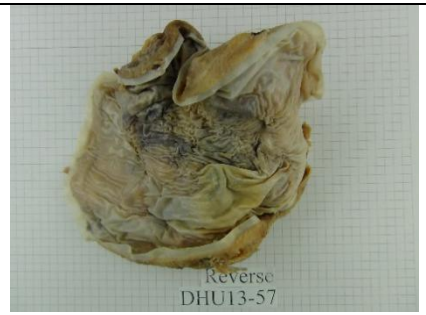	H: 19.60	H: 16.00	H: 18.37	482.16	165.83	65.61	152.44
			V: 24.60	V: 13.00	V: 47.15				

* The data are estimates.

Table S2A: Histology of the explanted devices: One layer of PP mesh

Code	Cross section	Histology		
DHU13-7 (141 days)	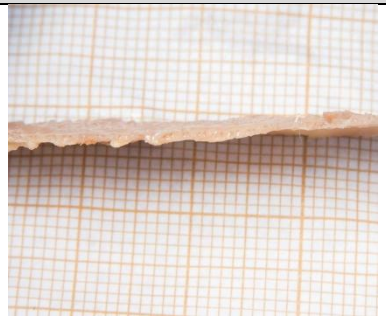	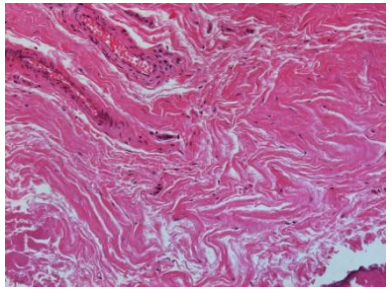	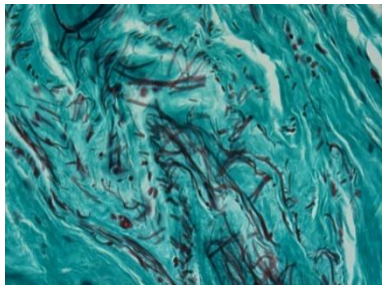	Widespread fibrosis with hyalinosis; moderate macrophage infiltration around the fabric; diffuse lymphocyte infiltration with haemorrhages; minimal giant cell reaction; foam cell occurrence; foci of necrosis; presence of fungi debris?
DHU13-10	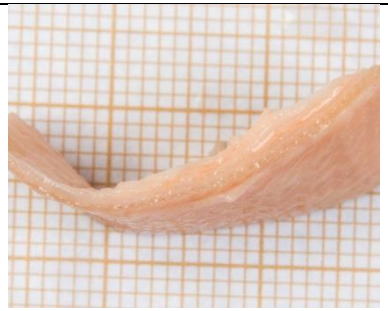	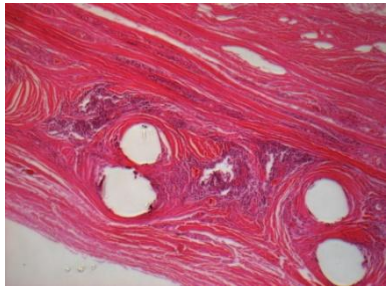	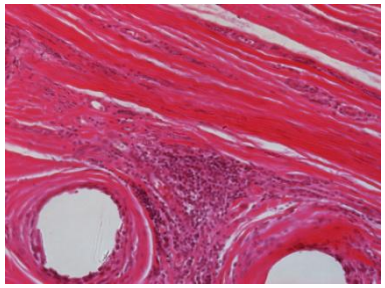	Fibrosis with perivascular macrophage and lymphocyte infiltration; moderate giant cell reaction; moderate outgrowth of granulations; some debris of fiber along the encapsulation.

Table S2B: Histology of the explanted device: Two layers of PP mesh

Code	Cross section	Histology		
DHU13-5 (1427 days)		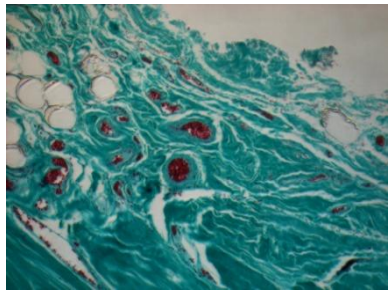	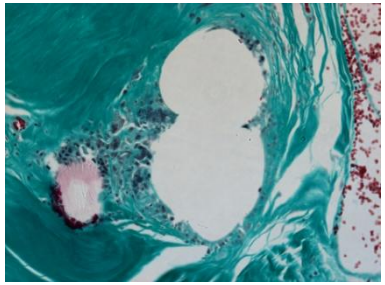	Widespread fibrosis with infiltration of macrophages low to moderate; Minimal giant cell reaction.

Table S2C: Histology of the explanted device: Two layers of PP mesh with 3-dimentional structure

Code	Cross section	Histology		
DHU13-52	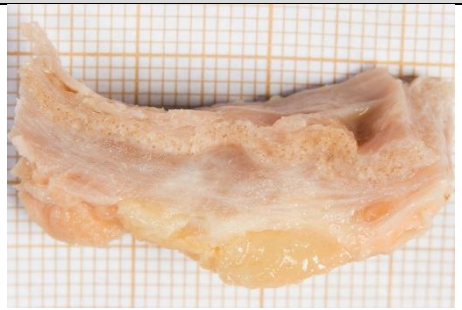	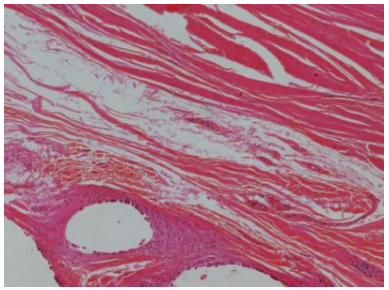	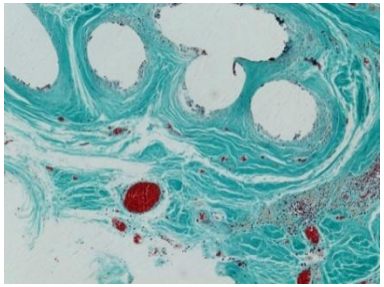	Significant fibrosis with macrophages and lymphocytes; moderate giant cell reaction and granulations.

Table S2D: Histology of the explanted device: Single ePTFE membrane

Code	Cross section	Histology		
DHU13-11 (1035 days)			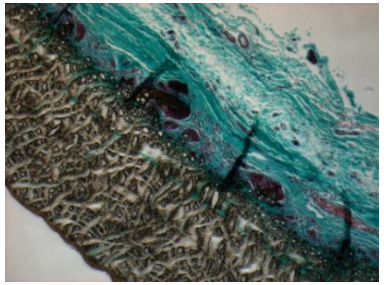	Intimate anchorage of the capsule with the ePTFE film and detachment of some nodule of the film within the fibrous capsul; very intensive giant cell reaction with fibrosis; Peri-implant macrophages and lymphocyte infiltration.

Table S2E: Histology of the explanted device: One layer of PP mesh + ePTFE membrane

Code	Cross section		Histology	
DHU13-13 (958 days)	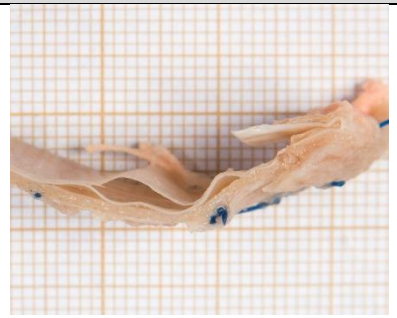	/	/	/

Table S2F(A) : Histology of the explanted devices: Two layers of PP mesh + ePTFE membrane

Code	Cross section	Histology		
DHU13-2 (1050 days)	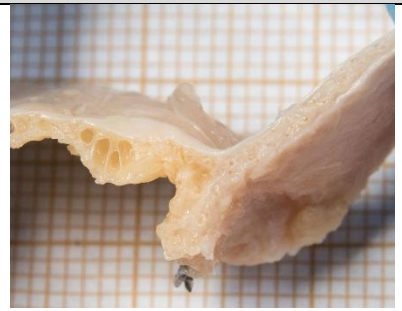	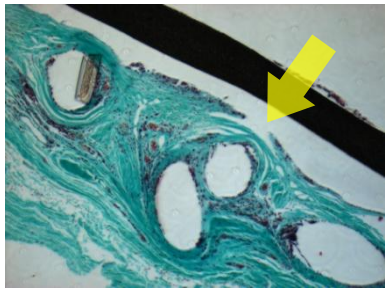	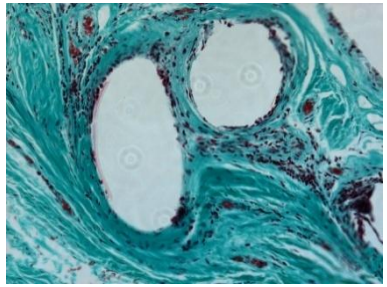	The PTFE is detached from the tissue encapsulated mesh (arrow); the fibrous capsule is infiltrated with minimal giant cells and lymphocytes around the textile fibers with evident fibrosis.
DHU13-4 (683 days)	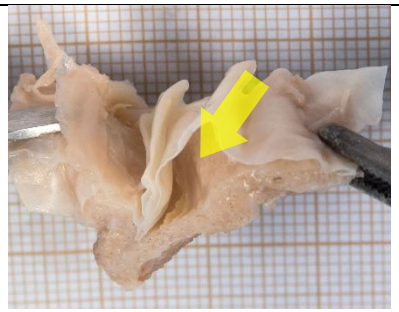	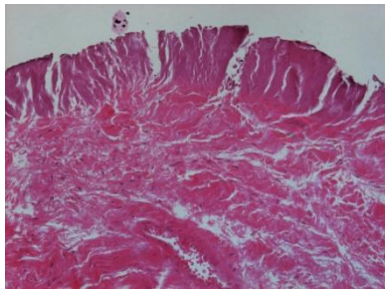	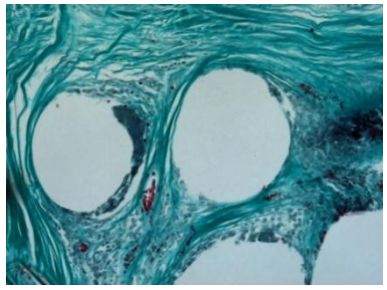	Thick fibrous layer with necrotized areas; Macrophage infiltration around the fibers of the fabric; visible presence of giant cell and leukocytes. Debris of fibers can connect with the tissue.

Table S2F(B) : Histology of the explanted devices: Two layers of PP mesh + ePTFE membrane

Code	Cross section	Histology		
DHU13-6 (600 days)		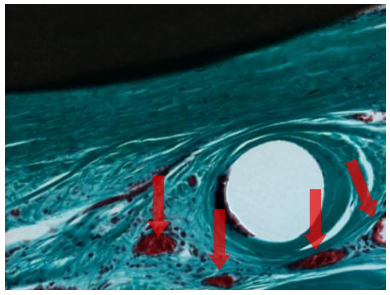	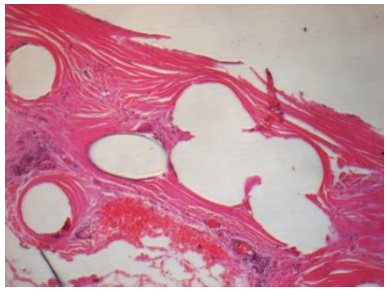	Poorly anchored film to the fibrous encapsulation of the fabric. Macrophages and lymphocytes are surrounding the textile fiber with debris of the polymer visible. Haemorrhages (arrows) and necrotized focci.

DHU13-57		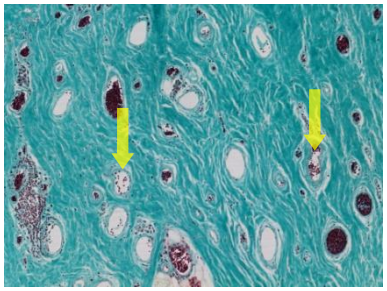	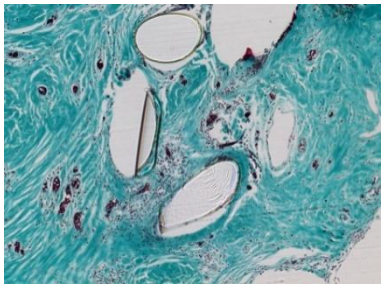	ePTFE film totally detached. Capsule with large fibrous areas. Significant lymphocyte infiltration surrounding the fiber of the fabric. Significant occurrence of granulation and necrotized areas (arrows).

Table S3A(A): SEM: single-layer PP

Code	Gross observations	SEM	
DHU13-3	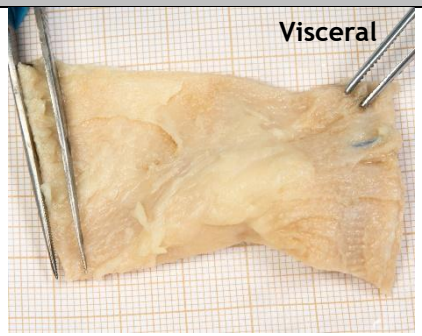	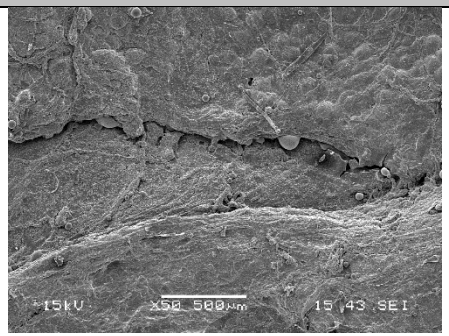	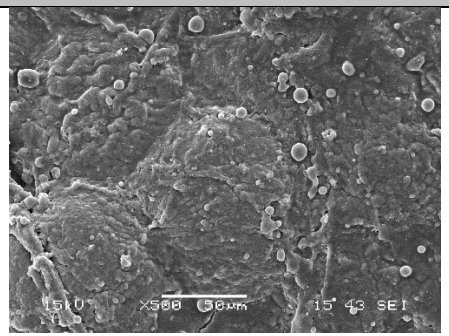
	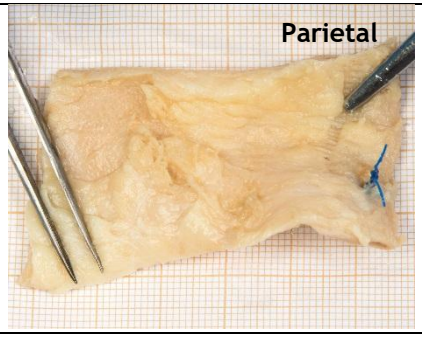	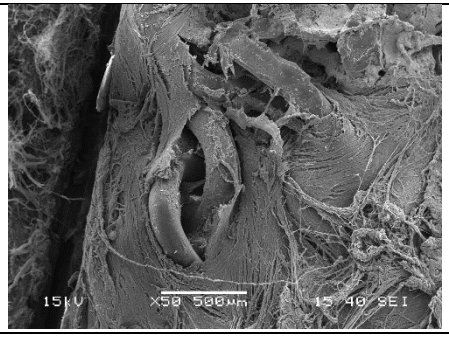	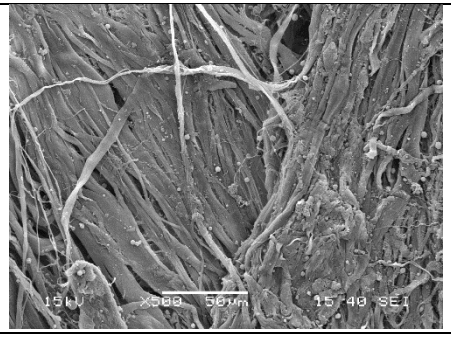

	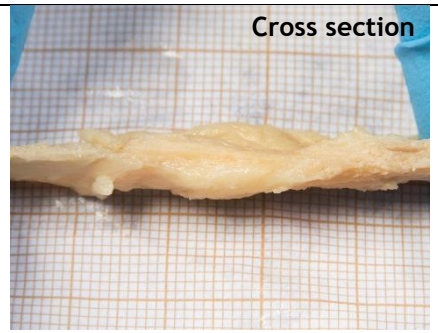	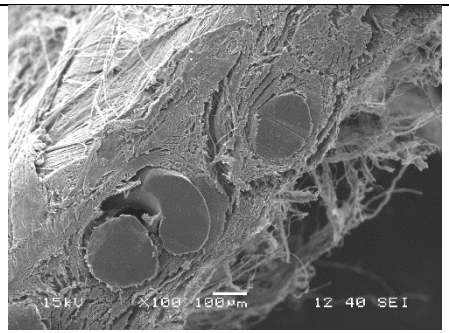	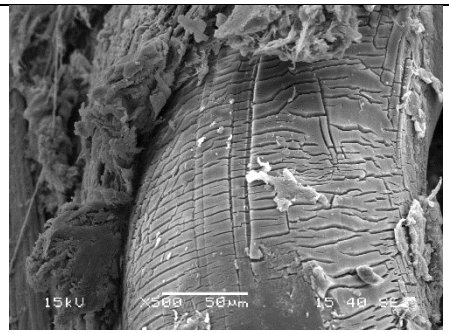

Table S3A(B): SEM: single-layer PP

Code	Gross observations	SEM	
DHU13-7 (141 days)	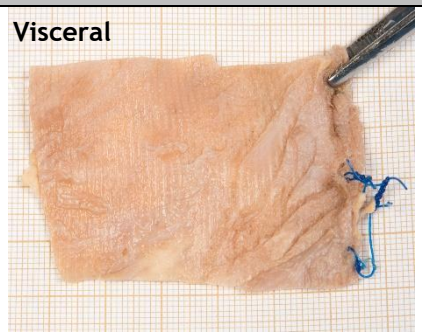	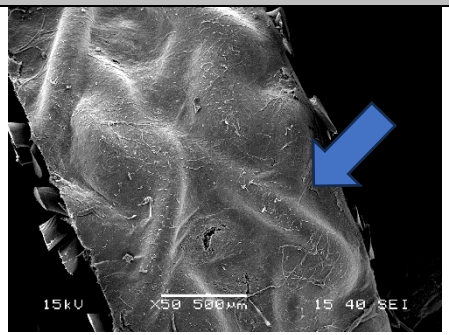	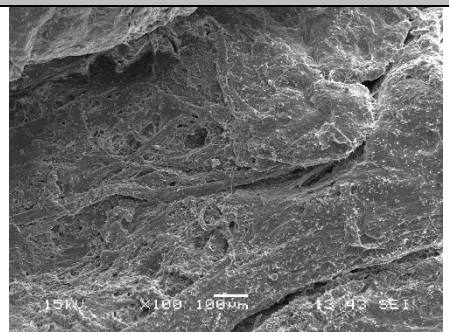
	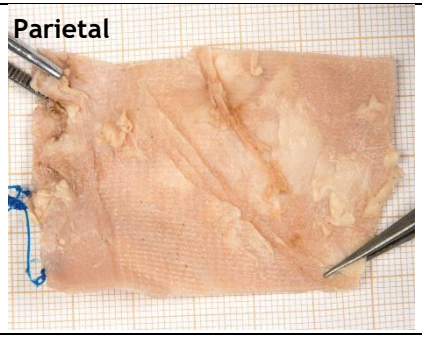	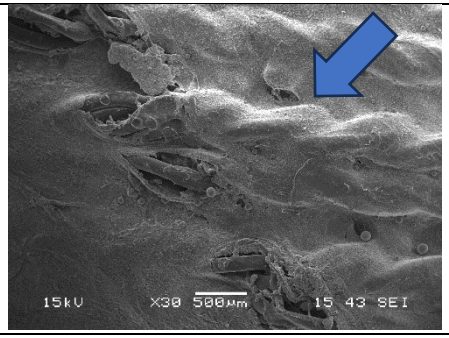	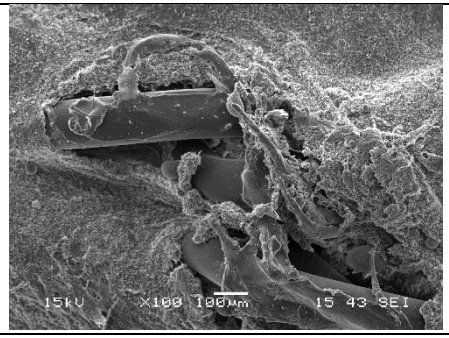

		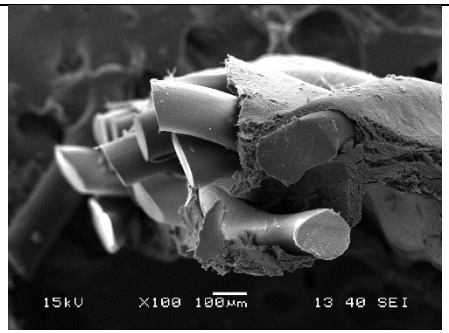	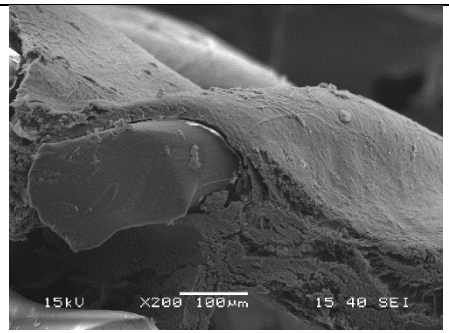

Table S3A(C): SEM: single-layer PP

Code	Gross observations	SEM	
DHU13-10	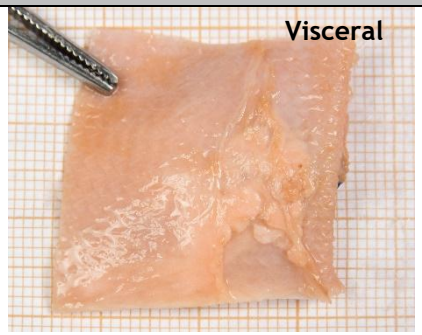	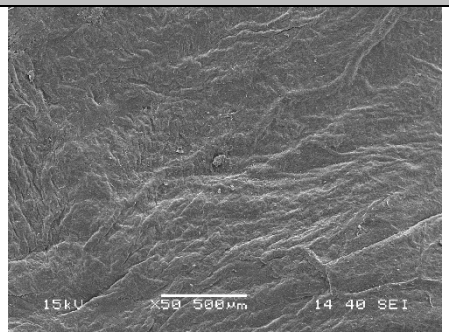	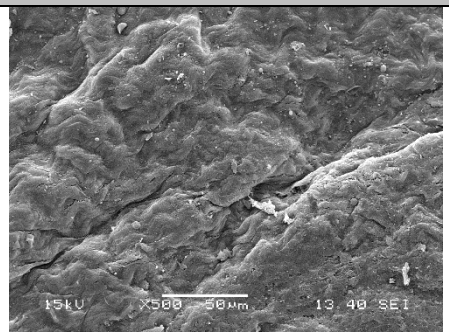
	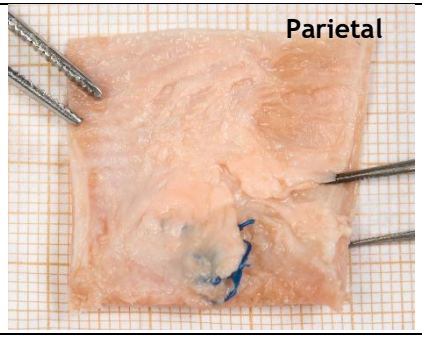	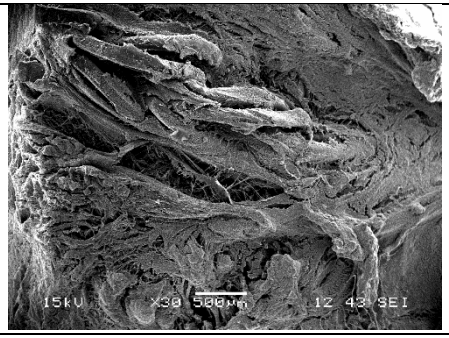	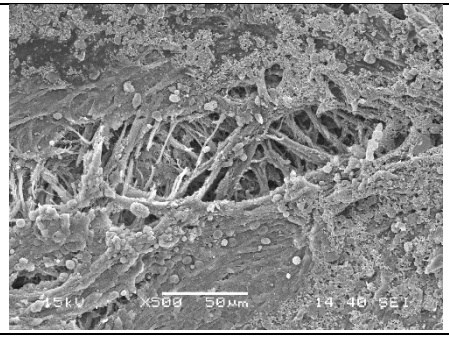

		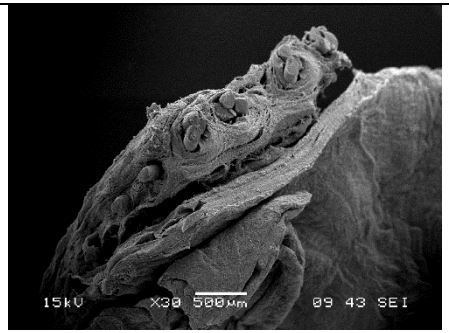	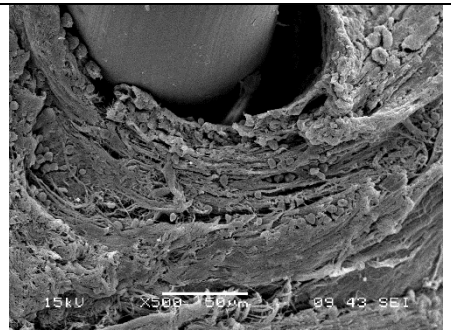

Table S3B: SEM: double-layer PP

Code	Gross observations	SEM	
DHU13-5 (1427 days)	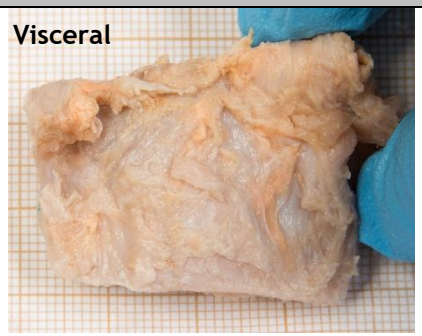	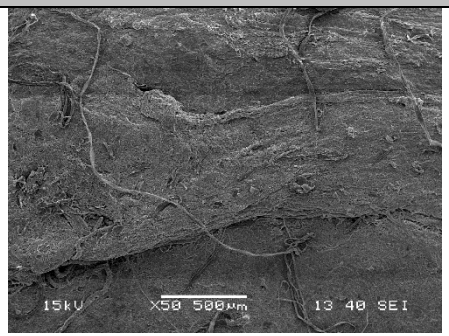	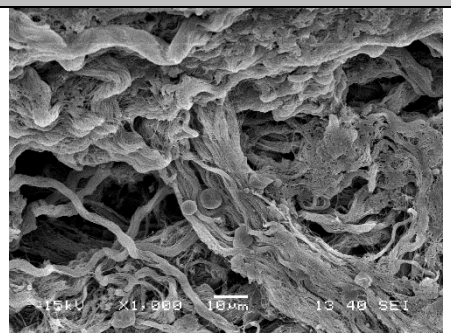
	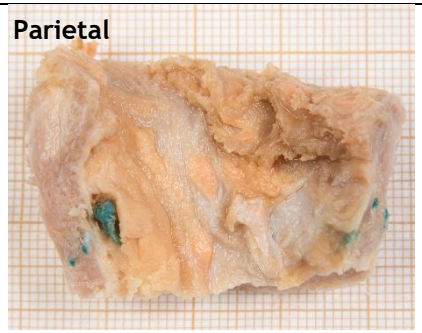	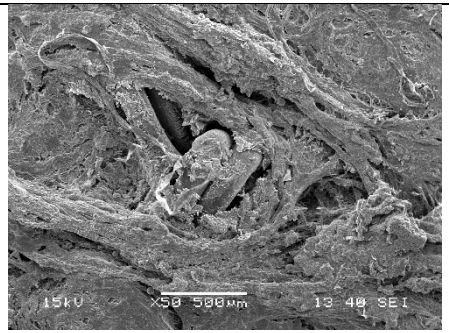	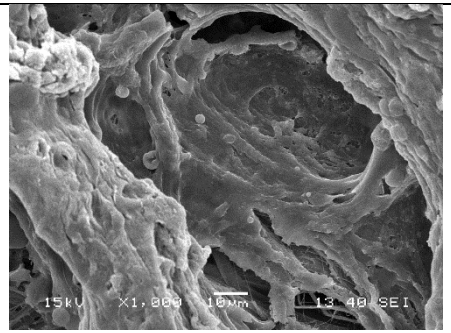

		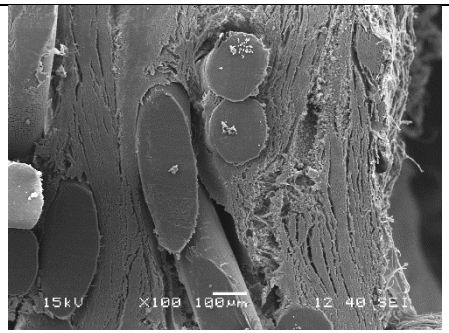	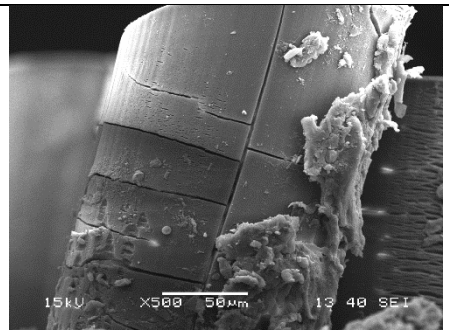

Table S3C: SEM: double-layer PP with 3-dimensional structure

Code	Gross observations	SEM	
DHU13-52	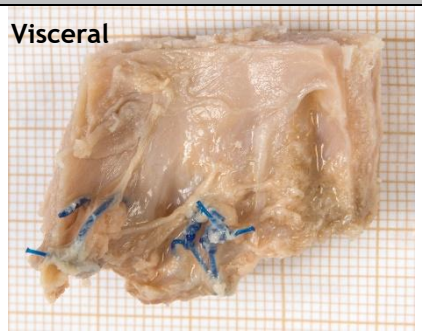	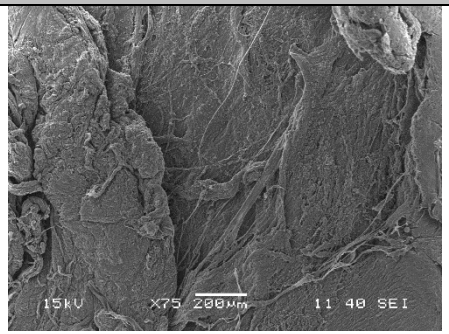	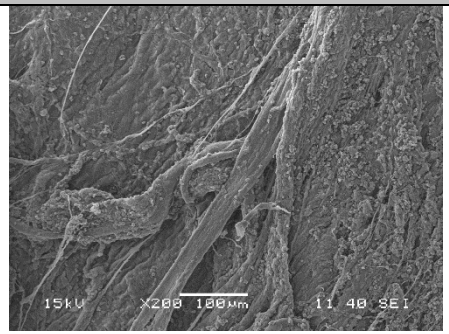
	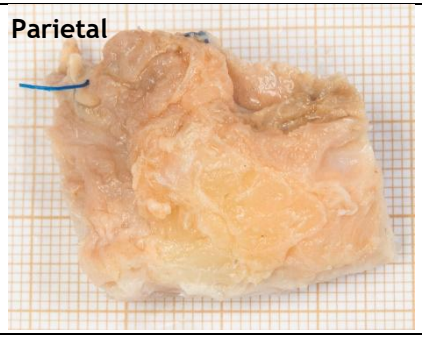	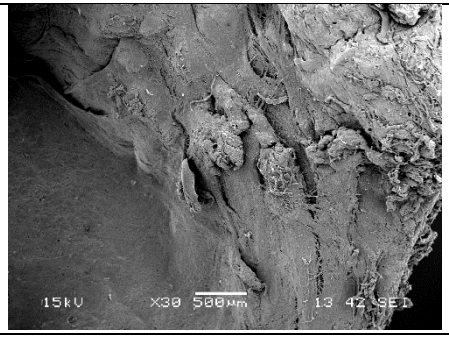	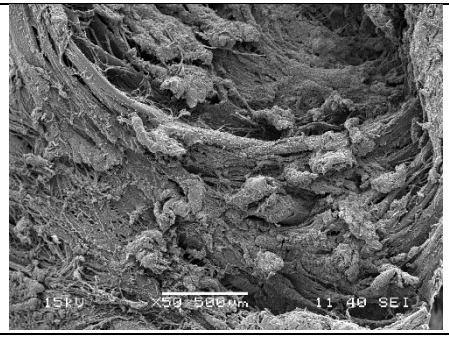

	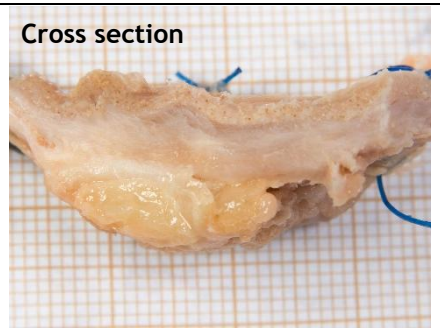	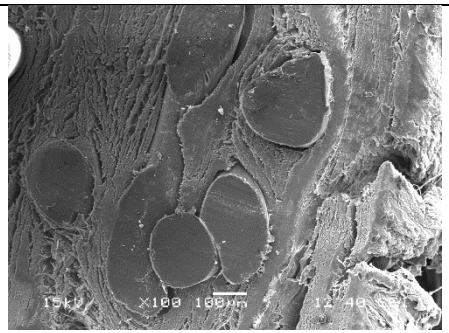	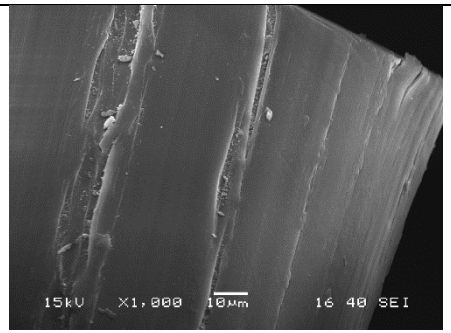

Table S3D: SEM: Single ePTFE membrane

Code	Gross observations	SEM	
DHU13-11 (1035 days)	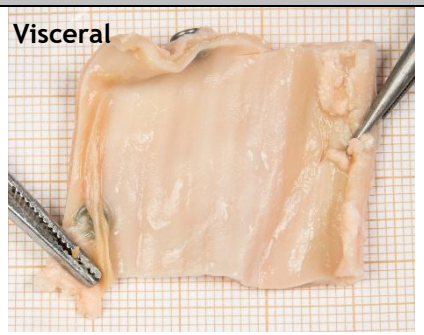	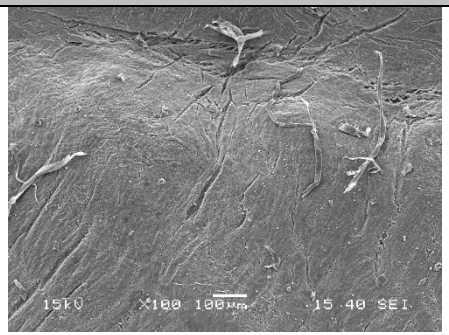	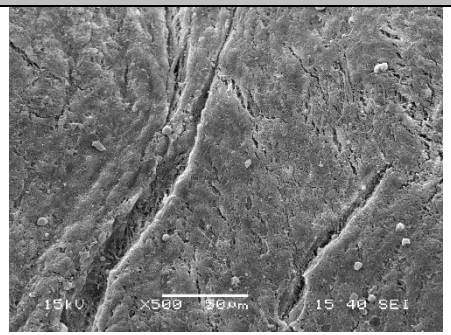
	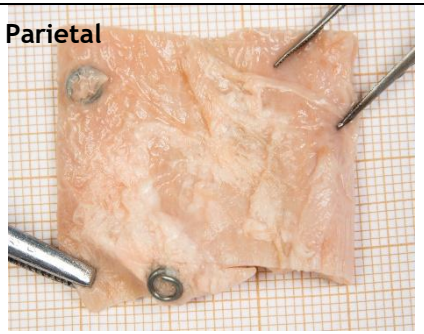	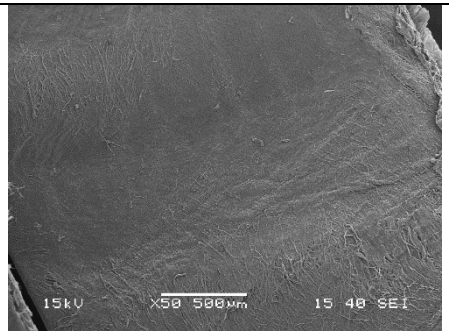	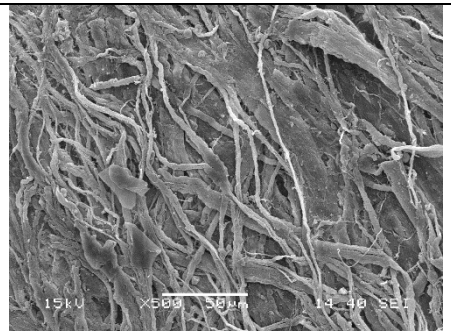

	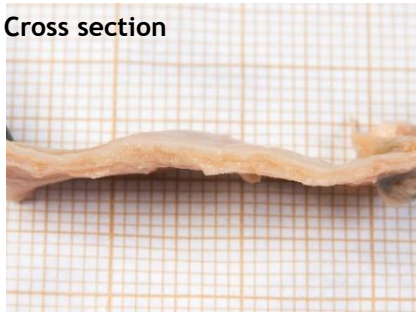	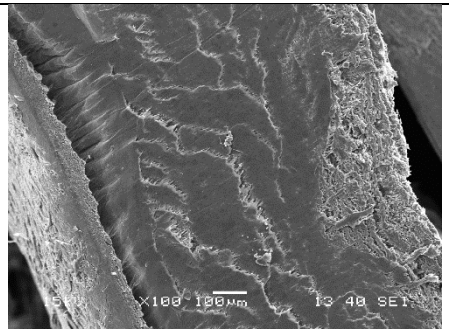	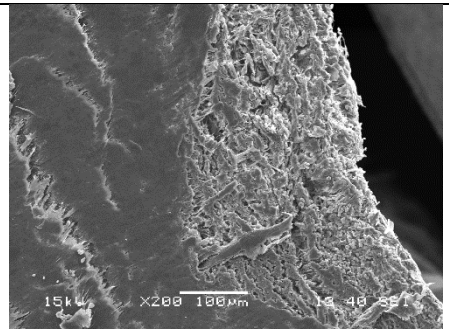

Table S3E: SEM: single-layer PP + ePTFE membrane

Code	Gross observations	SEM	
DHU13-13 (558 days)	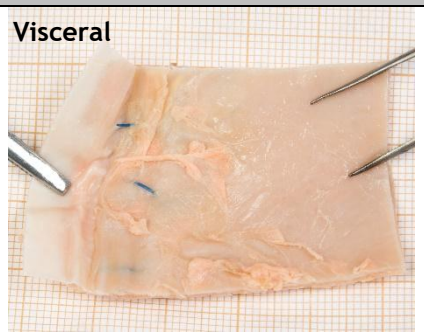	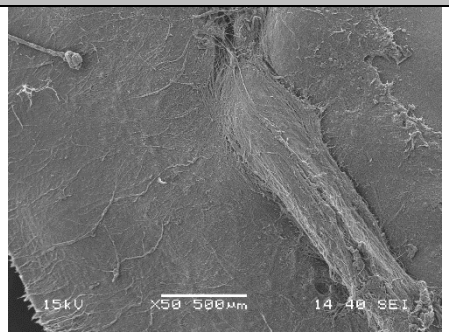	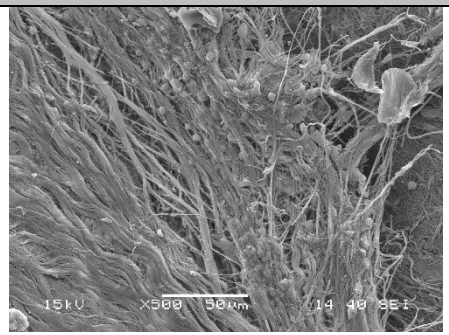
	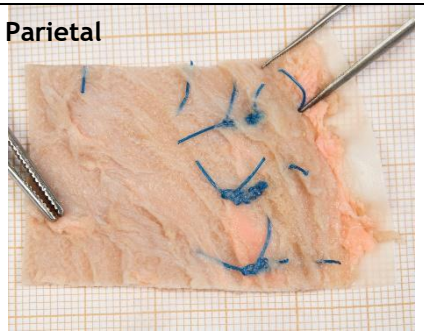	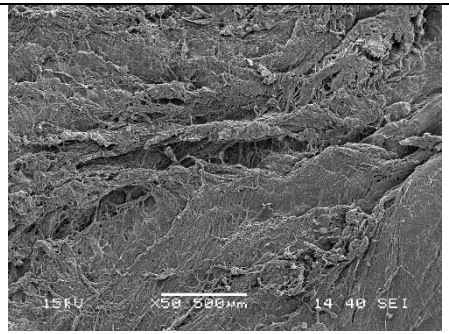	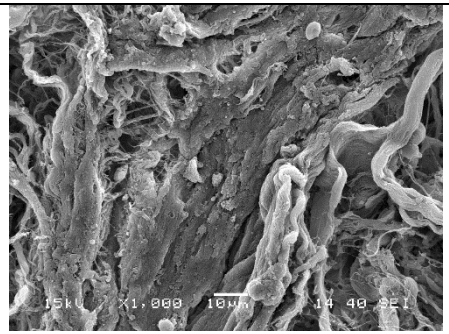

		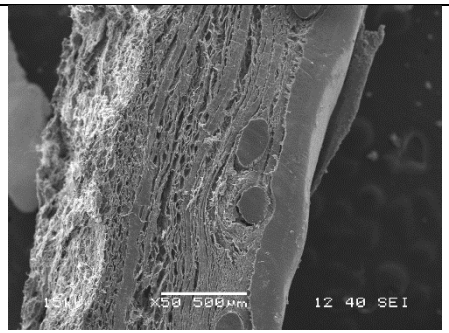	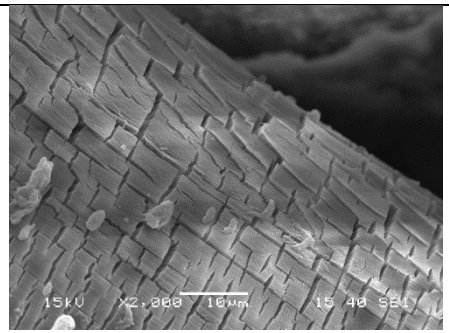

Table S3F(A): SEM: double-layer PP + ePTFE membrane

Code	Gross observations	SEM	
DHU13-2 (1050 days)	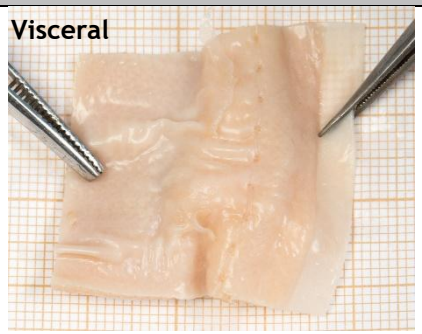	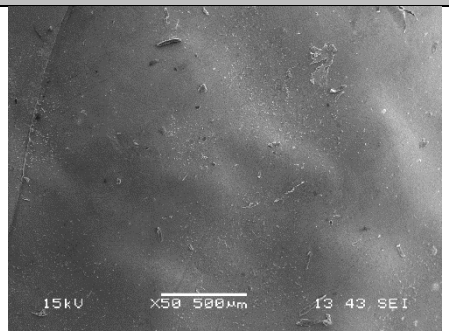	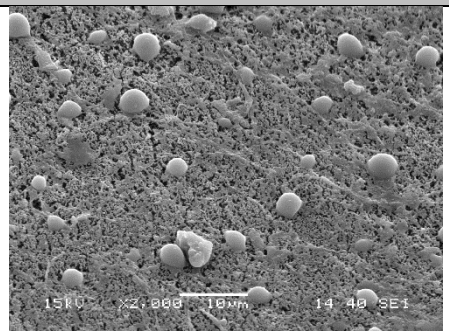
	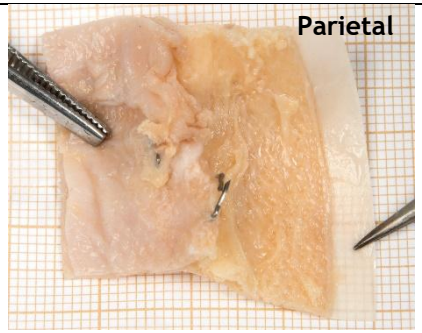	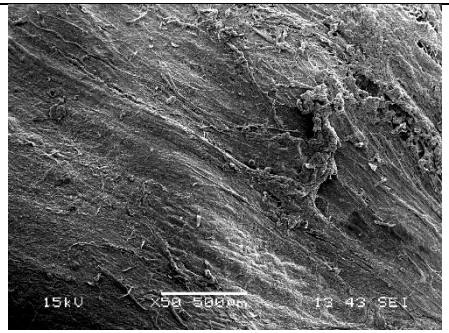	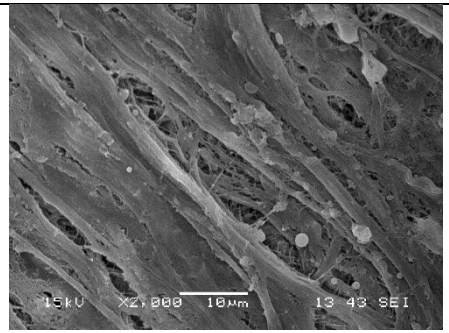

		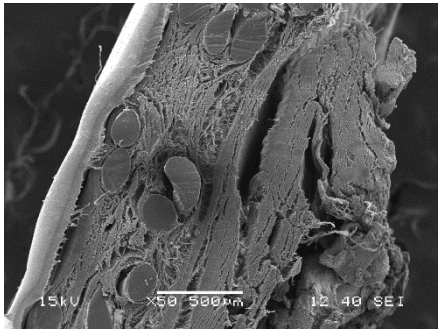	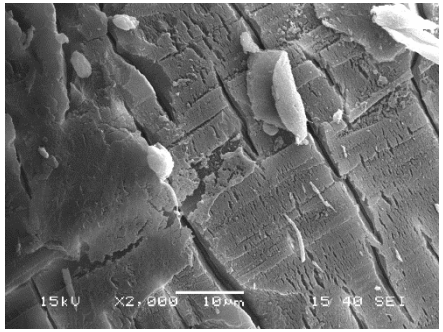

Table S3F(B): SEM: double-layer PP + ePTFE membrane

Code	Gross observations	SEM	
DHU13-4 (683 days)		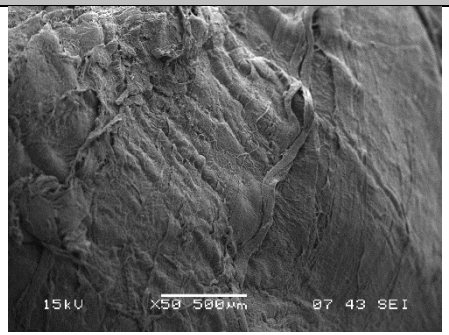	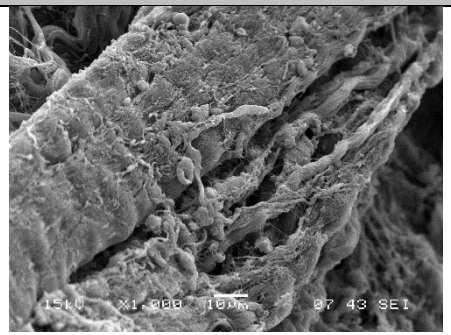
	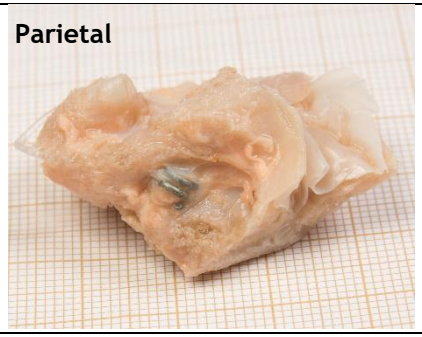	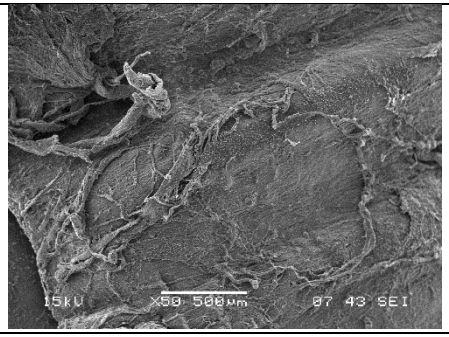	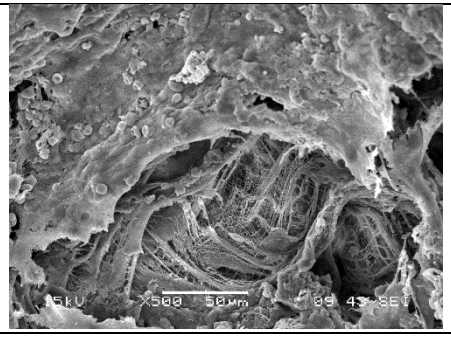

		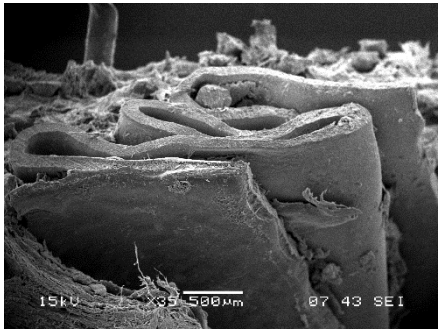	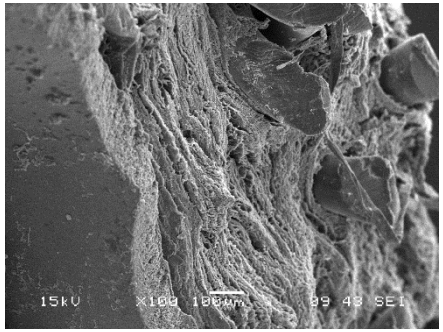

Table S3F(C): SEM: double-layer PP + ePTFE membrane

Code	Gross observations	SEM	
DHU13-6 (600 days)		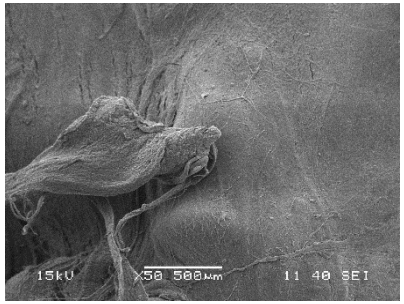	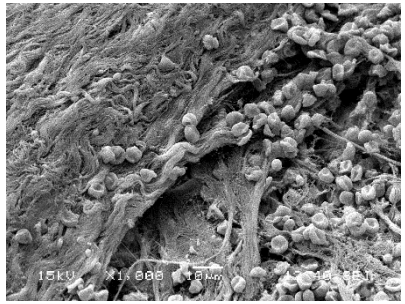
	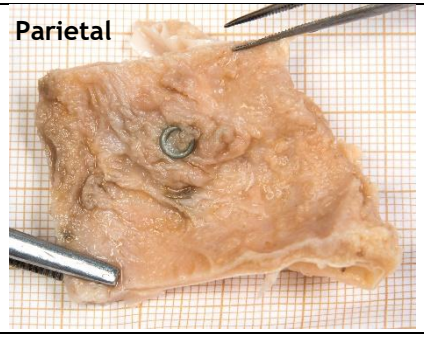	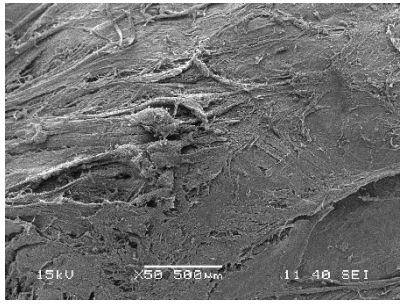	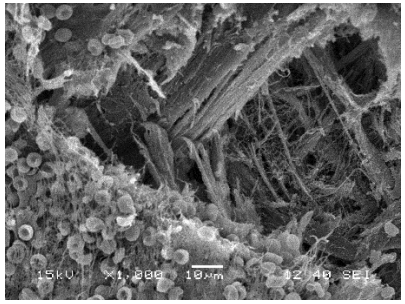

		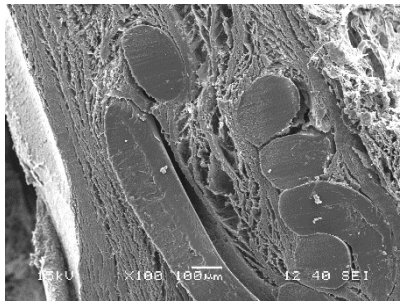	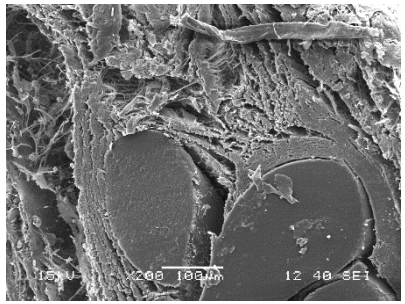

Table S3F(D) : SEM: double-layer PP + ePTFE membrane

Code	Gross observations	SEM	
DHU13-57	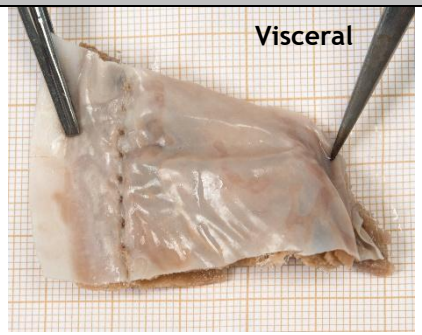	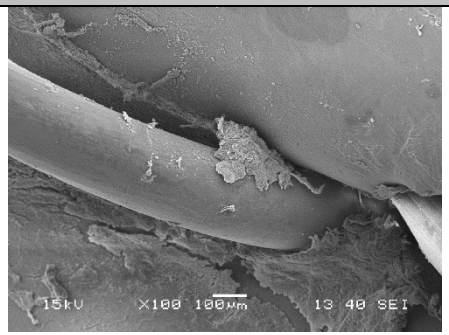	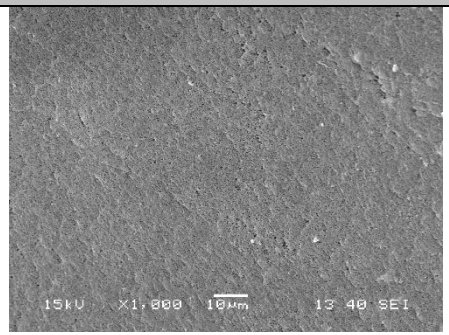
	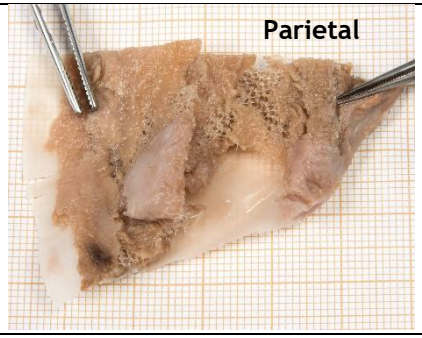	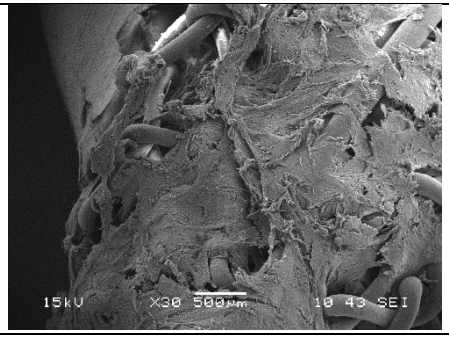	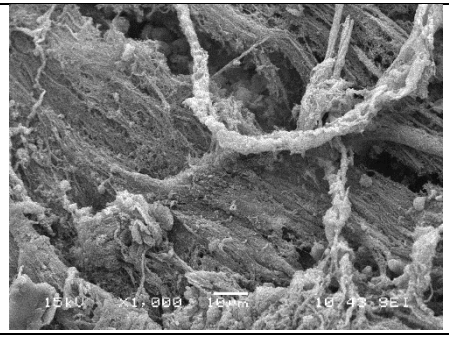

		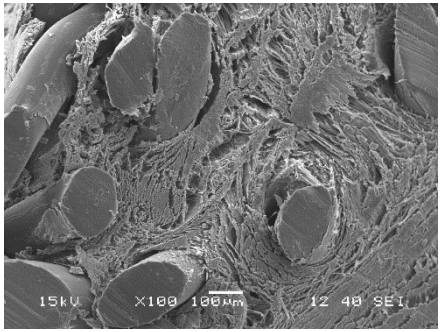	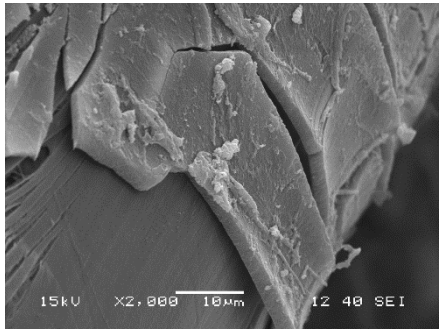

Table S4A: single-layer PP

Code	Gross observations	TEM		
DHU13-3	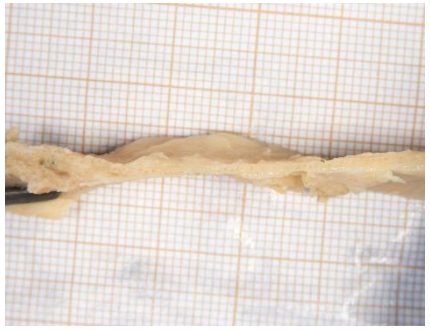	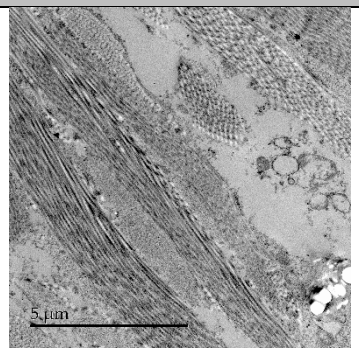	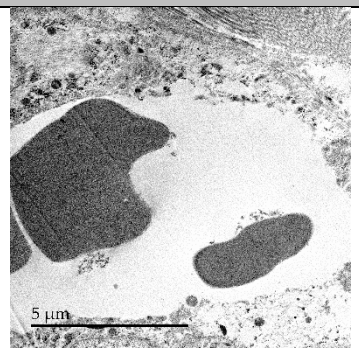	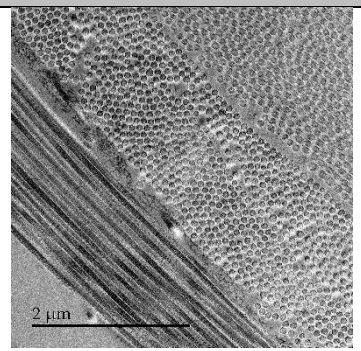
DHU13-7 (141 days)		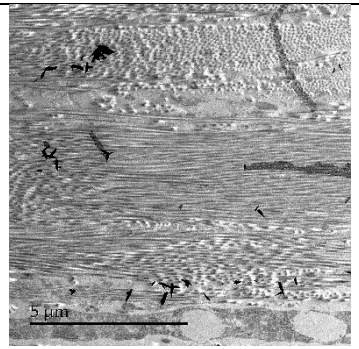	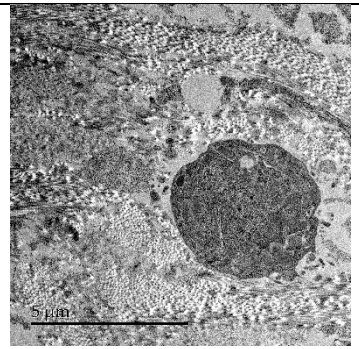	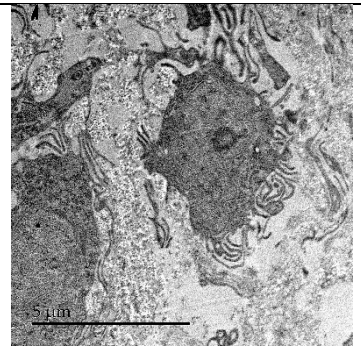

DHU13-10	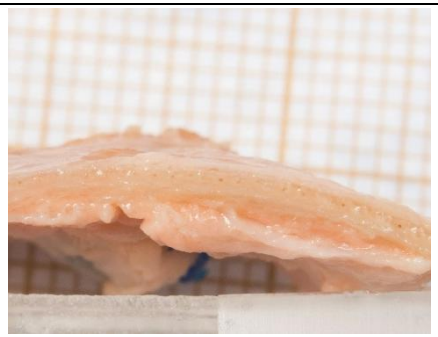	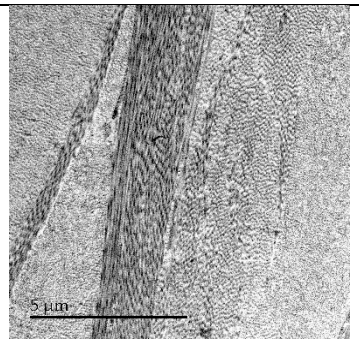	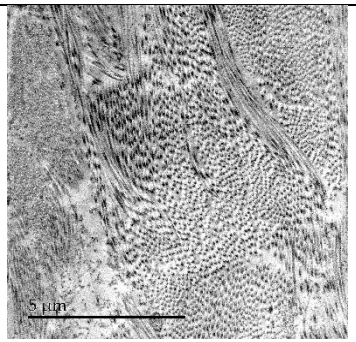	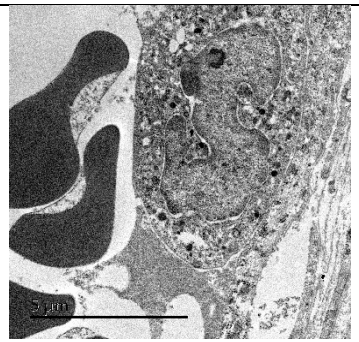

Table S4B : double-layer PP

Code	Gross observations	TEM		
DHU13-5 (1427 days)	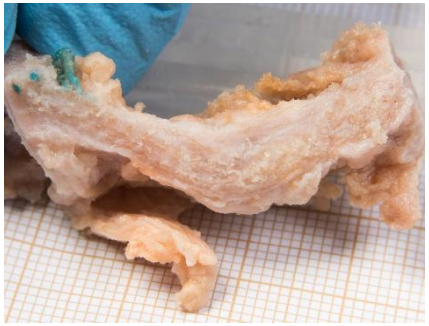	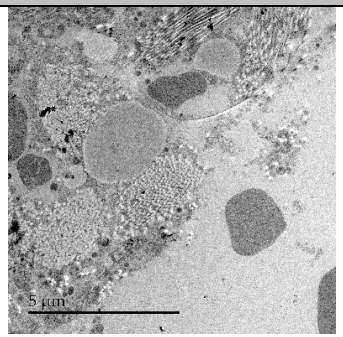	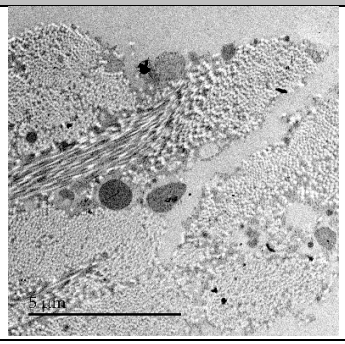	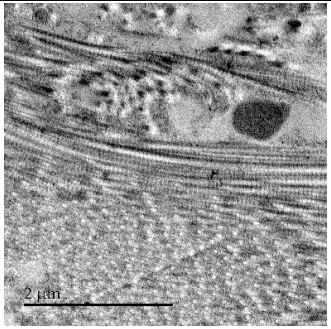

Table S4C: double-layer PP with 3-dimensional structure

Code	Gross observations	TEM		
DHU13-52	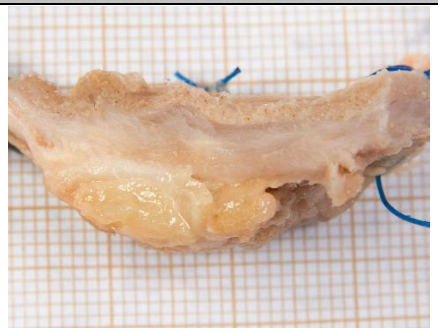	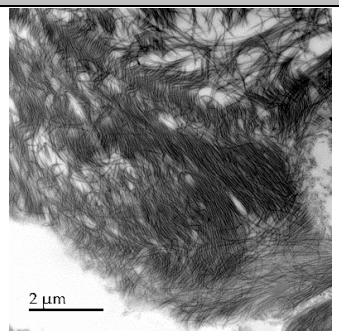	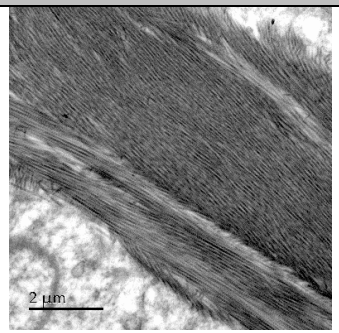	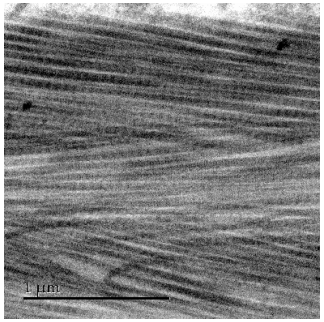

Table S4D: Single ePTFE membrane

Code	Gross observations	TEM	
DHU 13-11 (1035 days)		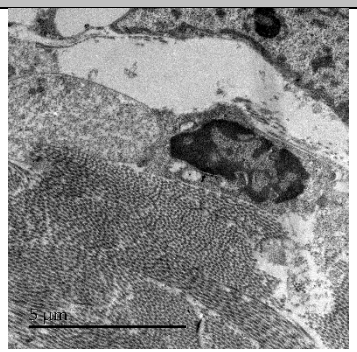	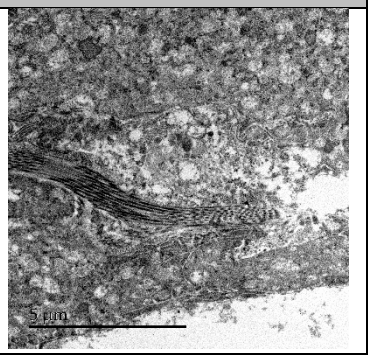

Table S4E: single-layer PP +ePTFE membrane

Code	Gross observations	TEM		
DHU13-13 (558 days)		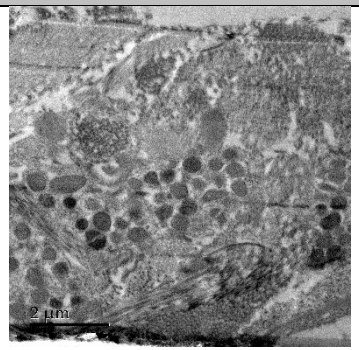	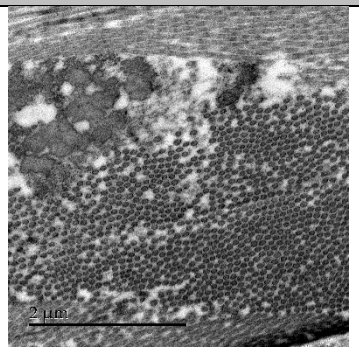	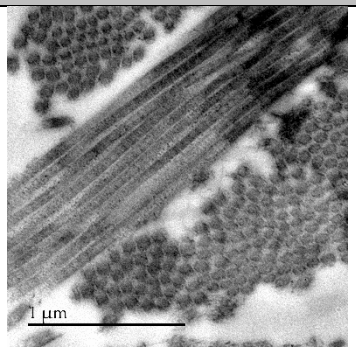

Table S4F(A): double-layer PP +ePTFE membrane

Code	Gross observations	TEM		
DHU13-2 (1050 days)	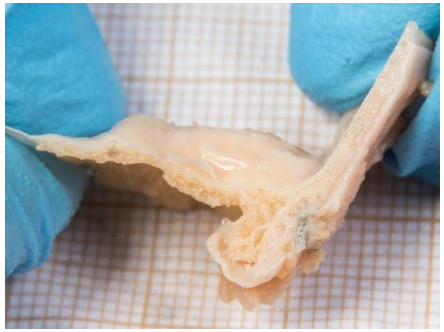	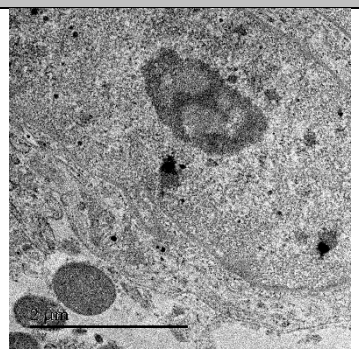	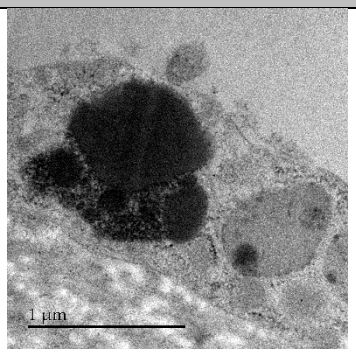	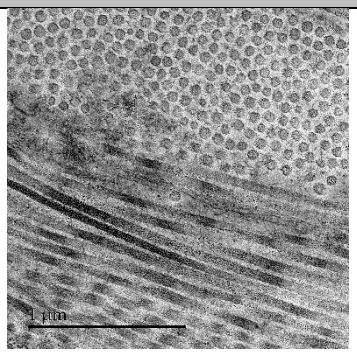
DHU13-4 (683 days)	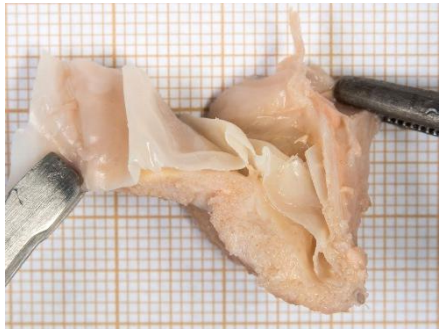	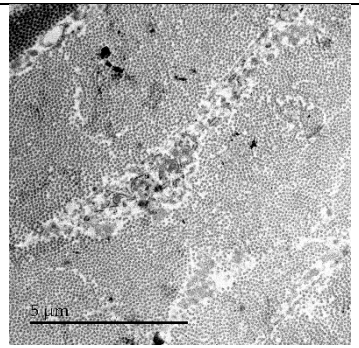	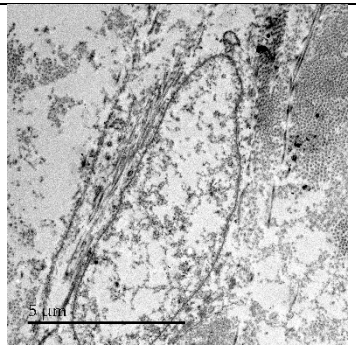	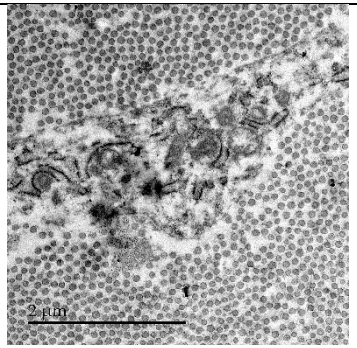

Table S4F(B) : double-layer PP +ePTFE membrane

Code	Gross observations	TEM		
DHU13-6 (600 days)	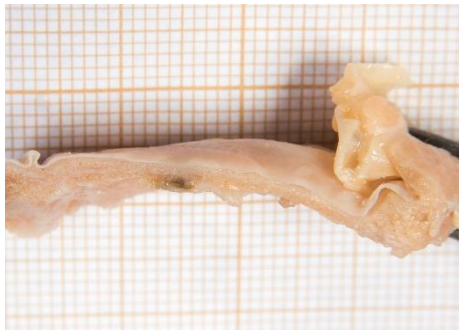	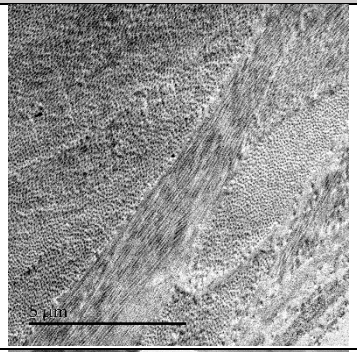		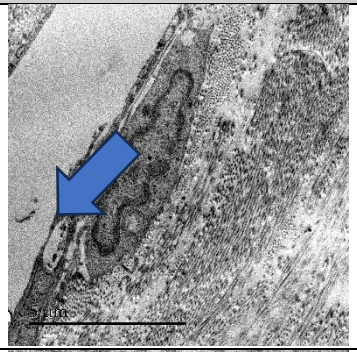
DHU 13-57	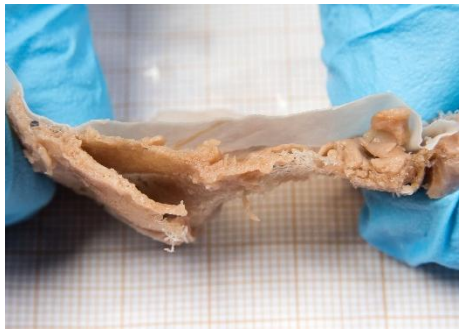	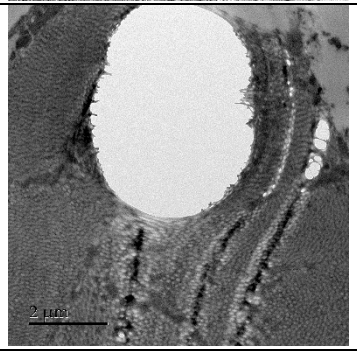	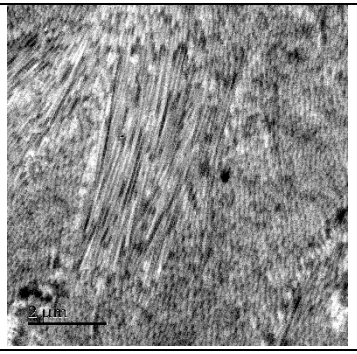	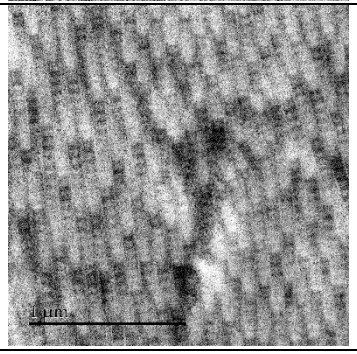

Table S5A: Morphology of the explanted devices after cleaning: single-layer PP

Code	Construction	Microscopy	SEM		
			100 X	500 X	1000 X
DHU 13-3	single-layer PP	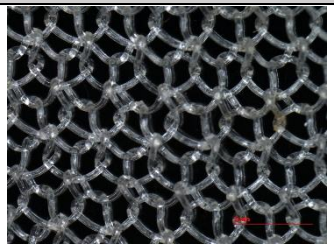	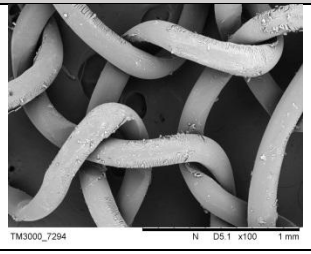	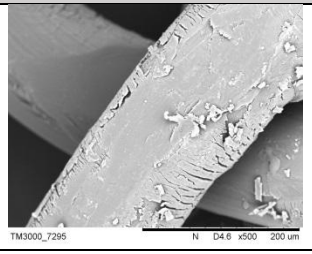	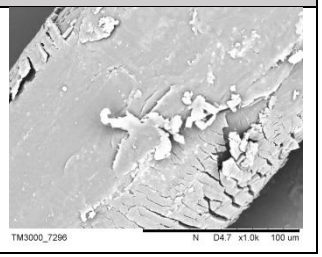

DHU13-7 (141 days)	single-layer PP	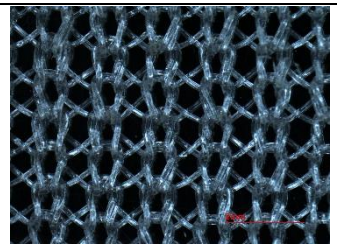	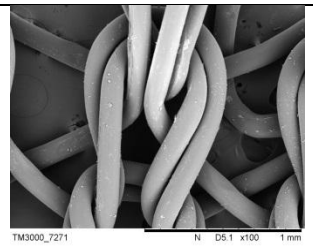	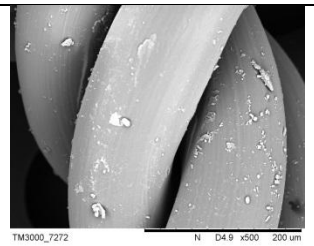	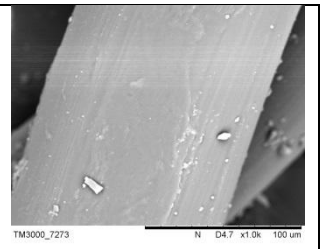
DHU13-10	single-layer PP	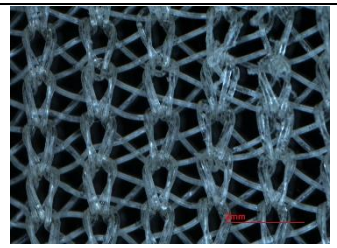	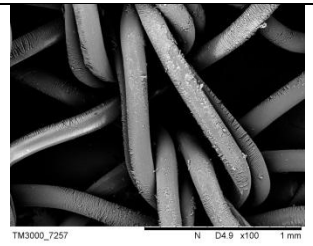	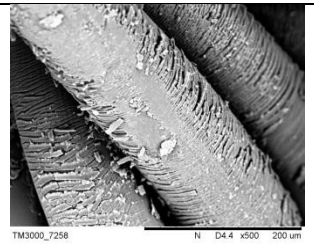	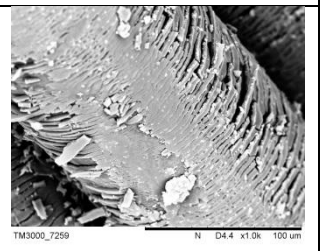

Table S5B: Morphology of the explanted device after cleaning: double-layer PP

Code	Construction	Microscopy	Morphology		
			100 X	500 X	1000 X
DHU13-5 (1427 days)	double-layer PP 1st layer	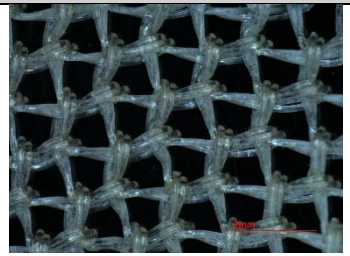	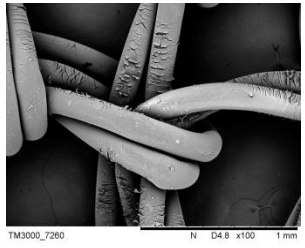	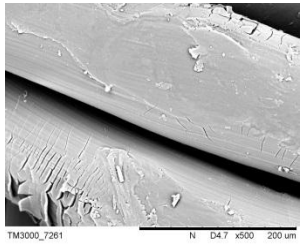	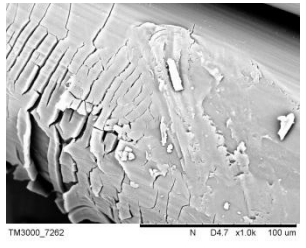
	2 layer PP 2nd layer	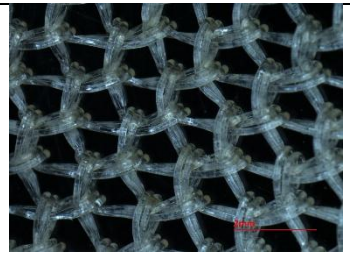	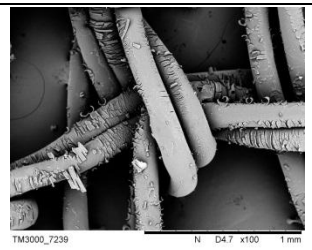	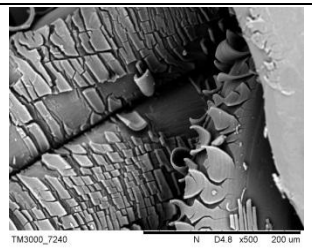	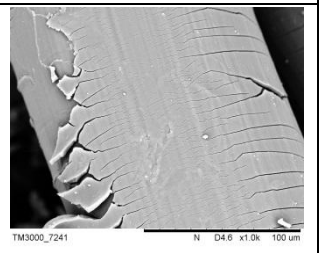

Table S5C : Morphology of the explanted device after cleaning: double-layer PP with 3-dimensional structure

Code	Construction	Microscopy	Morphology		
			100 X	500 X	1000 X
DHU13-52	double-layer PP 1st layer	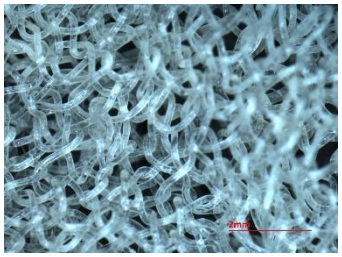		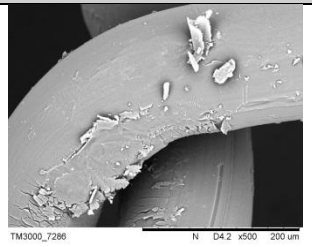	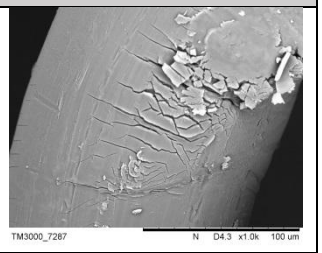
	2 layer PP 2nd layer		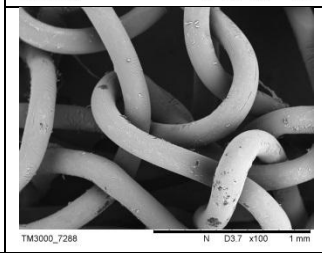	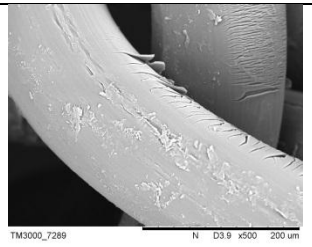	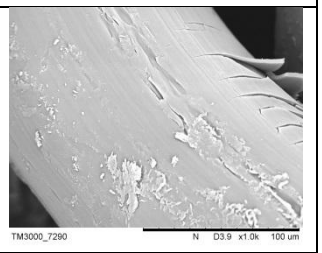

Table S5D : Morphology of the explanted device after cleaning : Single ePTFE membrane

Code	Construction	Microscopy	SEM		
			100 X	500 X	1000 X
DHU13-11 (1035 days)	ePTFE Membrane	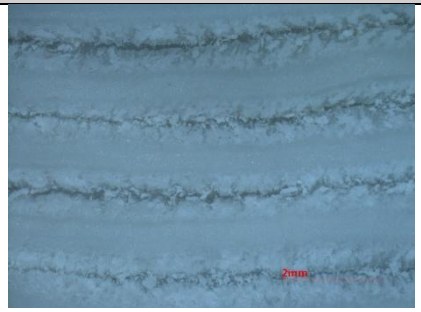	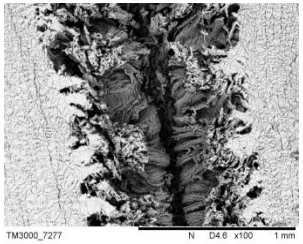	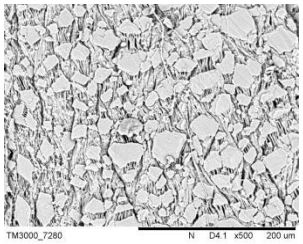	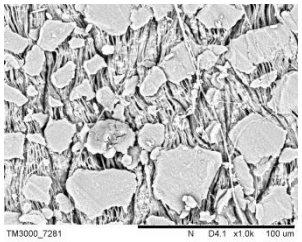

		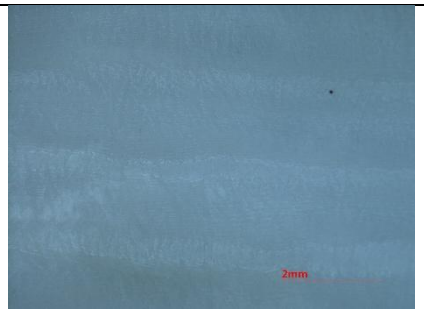		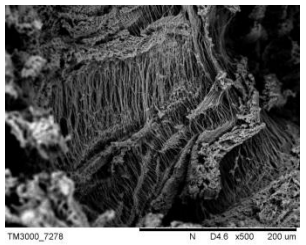	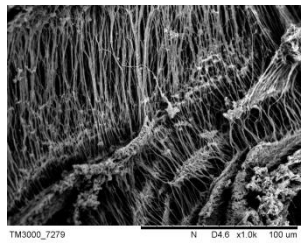

Table S5E : Morphology of the explanted device after cleaning: single-layer PP + 1 membrane ePTFE

Code	Construction	Microscopy	SEM		
			100 X	500 X	1000 X
DHU13-13 (558 days)	single-layer PP	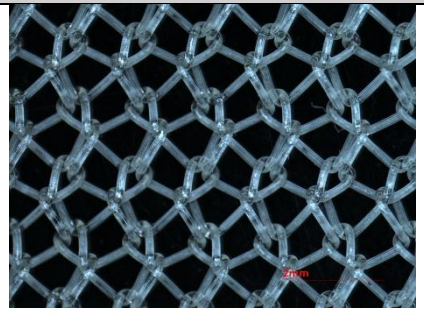	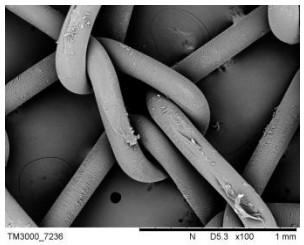	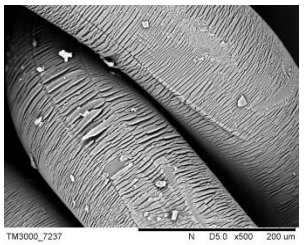	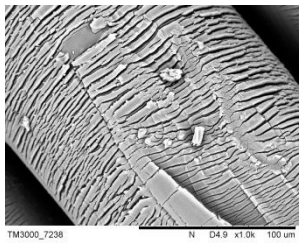
	ePTFE Membrane	/	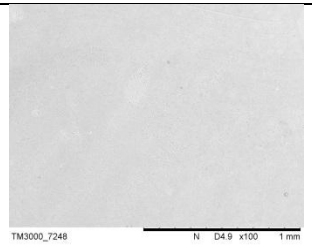	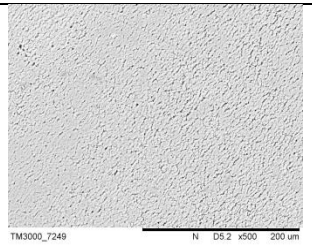	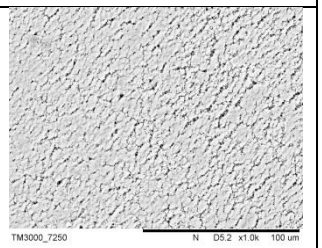

Table S5F (A): Morphology of the explanted device after cleaning double-layer PP + 1 membrane ePTFE

Code	Construction	Microscopy	SEM		
			100 X	500 X	1000 X
DHU13-2 (1050 days)	1st layer PP	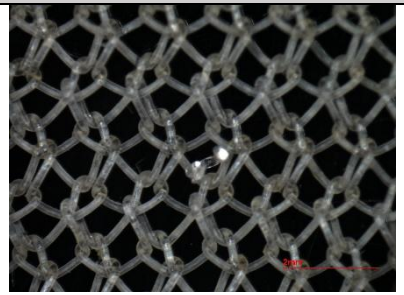	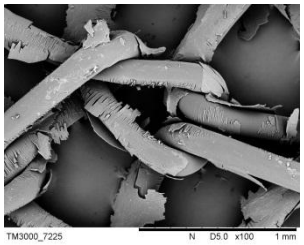	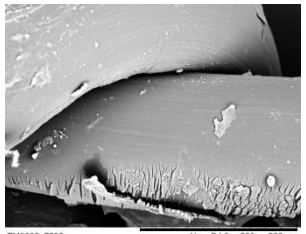	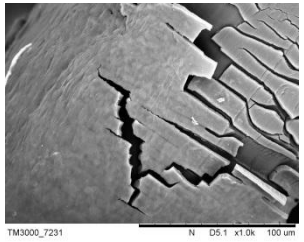
	2nd layer PP	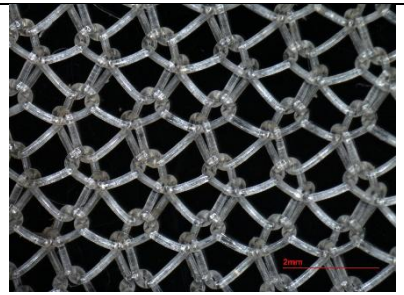	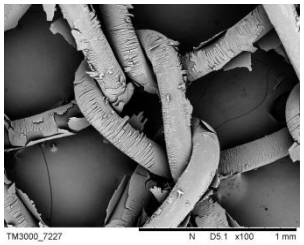	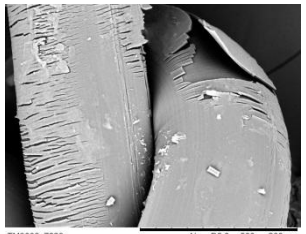	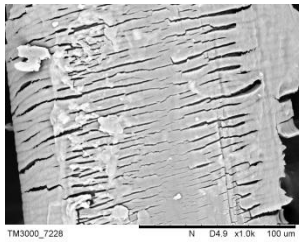
	ePTFE Membrane	/	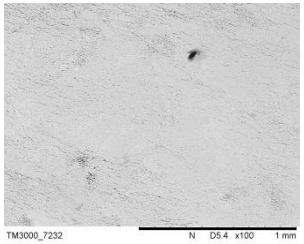	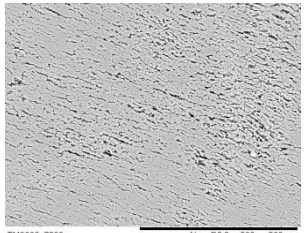	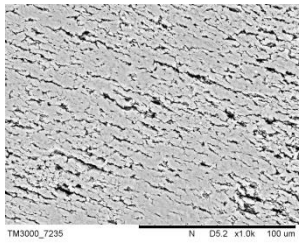

Table S5F (B): Morphology of the explanted device after cleaning : double-layer PP + ePTFE membrane

Code	Construction	Microscopy	SEM		
			100 X	500 X	1000 X
DHU13-4 (683 days)	1st layer PP	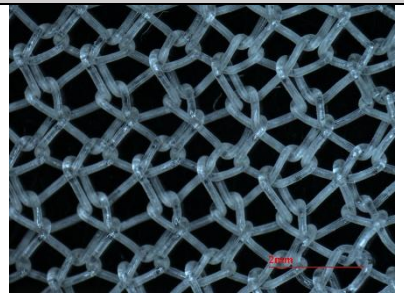	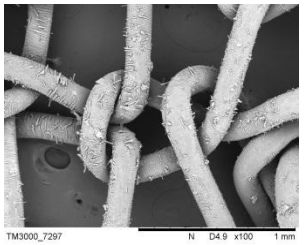	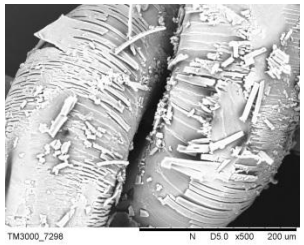	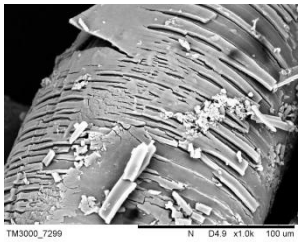
	2nd layer PP	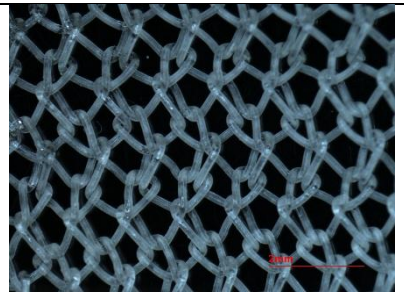		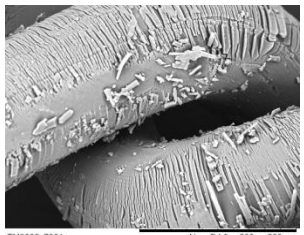	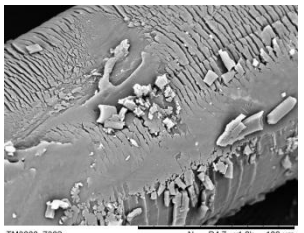
	ePTFE Membrane	/	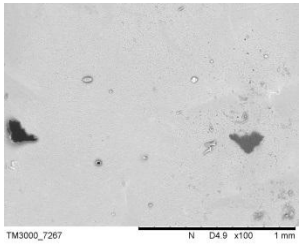	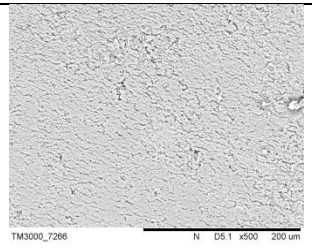 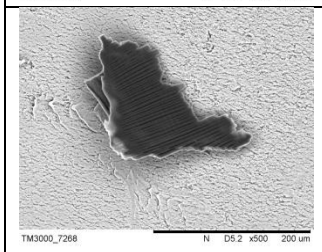	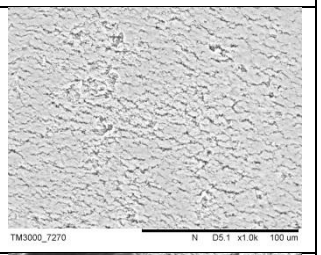 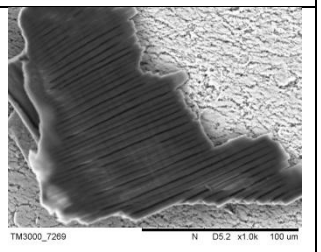

Table S5F(C): Morphology of the explanted device after cleaning double-layer PP + 1 membrane ePTFE

Code	Construction	Microscopy	SEM		
			100 X	500 X	1000 X
DHU13-6 (600 days)	1st layer PP	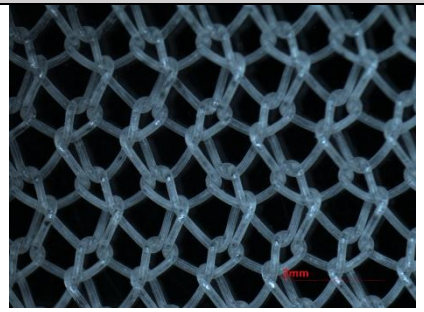	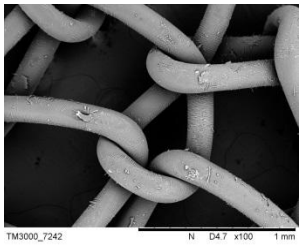	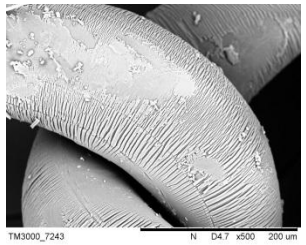	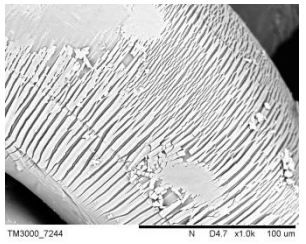
	2nd layer PP	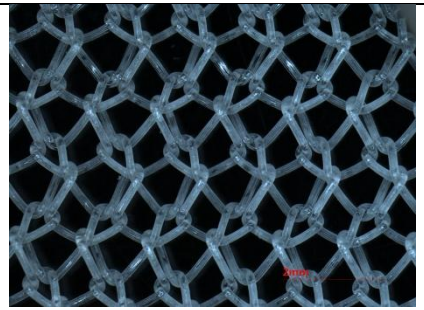	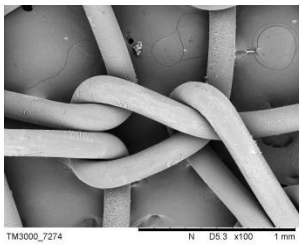	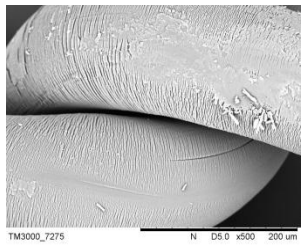	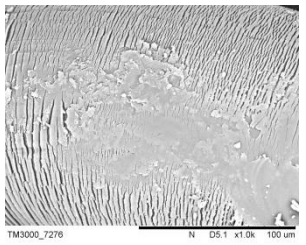
	ePTFE Membrane	/	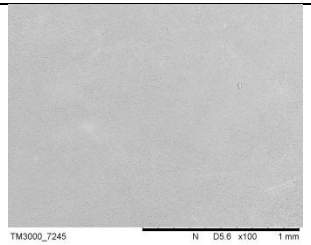	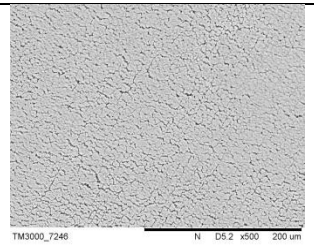	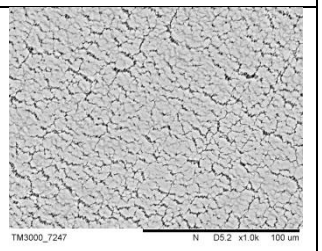

Table S5F(D): Morphology of the explanted device after cleaning : double-layer PP + ePTFE

Code	Construction	Microscopy	SEM		
			100 X	500 X	1000 X
DHU13-57	1st layer PP	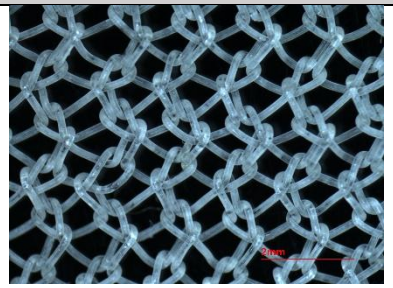	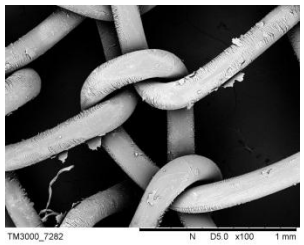	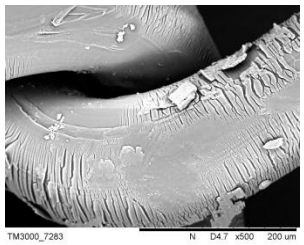	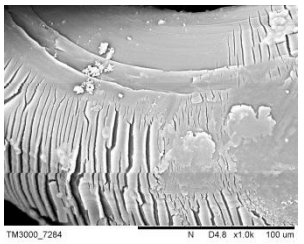
	2nd layer PP	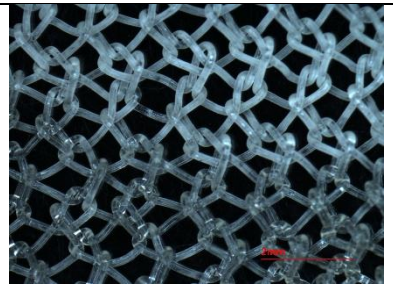	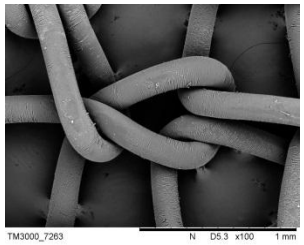	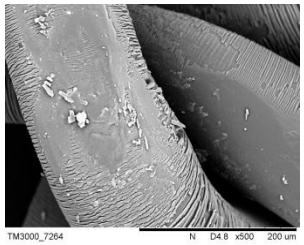	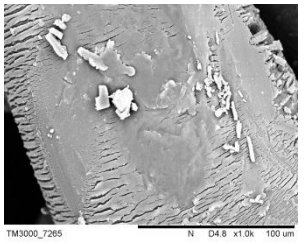
	ePTFE Membrane	/	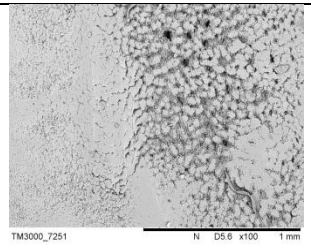	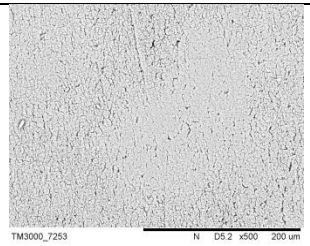	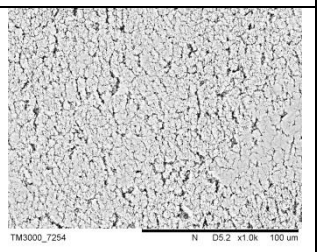
		/	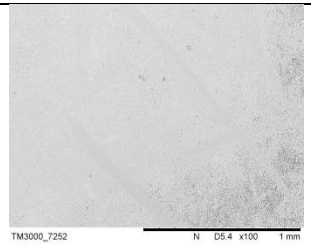	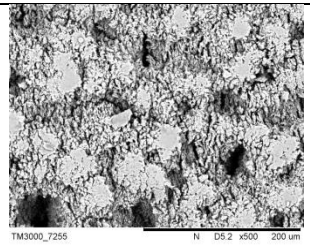	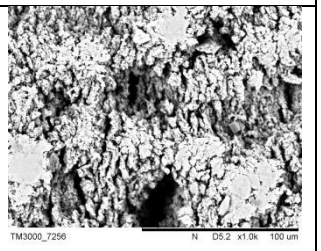

Table S6A: Physical characteristics

Code	Construction	Sections	Thickness (mm)	Weight/ Surface unit (g/m^2)	Filament diameter (mm)	Porosity (%)
DHU13-3	single-layer PP	First layer	0.6488±0.0223	87.6129	0.1821±0.0090	37.34±0.55
DHU13-7 (141 days)		Mesh	0.5530±0.0047	107.6948	0.1419±0.0012	33.26±1.38
DHU13-10		Mesh	0.7478±0.0413	119.0192	0.1444±0.0040	32.61±1.83
DHU13-5 (1427 days)	double-layer PP	First layer	0.7276±0.0411	117.1881	0.1731±0.0048	37.74±0.91
		Second layer	0.7406±0.0207	93.1369	0.1714±0.0042	36.68±0.91
DHU13-52	double-layer PP with 3-dimensional structure	Mesh	1.8220±0.0640	259.5474	0.1742±0.0039	/
DHU13-11 (1035 days)	Single ePTFE membrane	Membrane	1.1812±0.0686	1113.8574	/	/
DHU13-13 (558 days)	single-layer PP +ePTFE membrane	First layer	0.5898±0.0055	98.8922	0.1751±0.0081	46.46±1.59
		Second layer	0.2082±0.0102	251.8163	/	/

Table S6B: Physical characteristics

Code	Construction	Sections	Thickness (mm)	Weight/ Surface unit (g/m^2)	Filament diameter (mm)	Porosity (%)
DHU13-2 (1050 days)	double-layer PP +ePTFE membrane	First layer	0.5820±0.0082	93.7907	0.1822±0.0103	40.93±1.93
		Second layer	0.5490±0.0091	76.1428	0.1684±0.0063	44.55±1.59
		Membrane	0.1734±0.0107	186.9164	/	/
DHU13-4 (683 days)		First layer	0.6042±0.0195	104.2580	0.1705±0.0031	40.33±2.52
		Second layer	0.6242± 0.0213	115.1196	0.1691±0.0042	37.77±1.44
		Membrane	0.1906±0.0102	233.0833	/	/
DHU13-6 (600 days)		First layer	0.5494±0.0145	79.7903	0.1739±0.0051	46.24±1.02
		Second layer	0.5696±0.0042	88.7566	0.1726±0.0039	45.57±0.25
		Membrane	0.1610±0.0080	180.1481	/	/
DHU13-57		First layer	0.6248±0.0163	94.0917	0.1724±0.0022	39.57±0.83
		Second layer	0.6256±0.0173	120.8680	0.1681±0.0051	39.72±0.81
		Membrane	0.3116±0.0145	222.5853	/	/

Table S7A: Chemistry: One layer of PP mesh

Code	Sections	SEM 500 X	ATR-FTIR	DSC
DHU13-3	Mesh	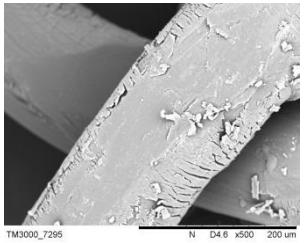	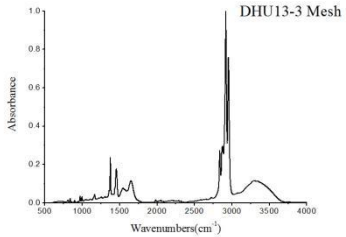	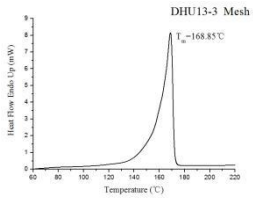
DHU13-7	Mesh	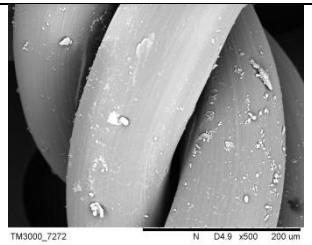	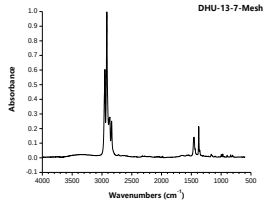	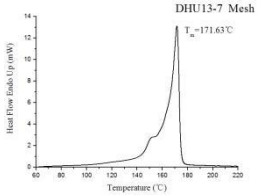
DHU13-10	Mesh	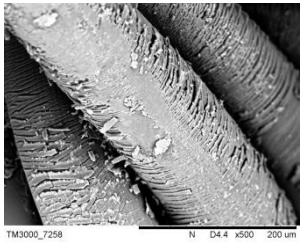	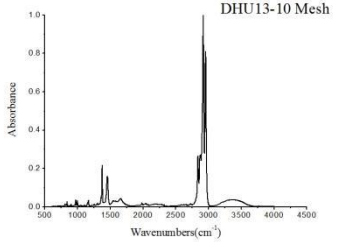	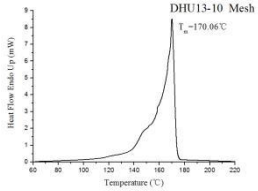

Table S7B: Chemistry: Two layers of PP mesh

Code	Sections	SEM 500 X	ATR-FTIR	DSC
DHU13-5 (1427 days)	First layer	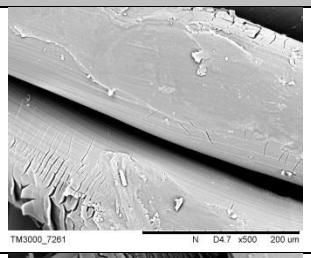	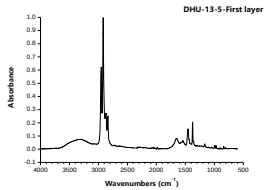	/
	Second layer	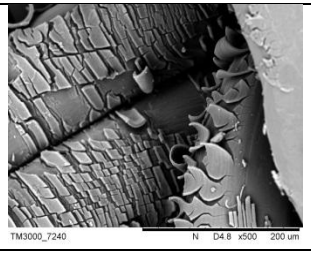	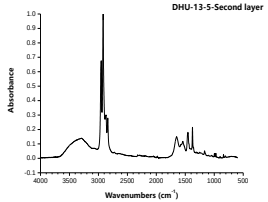	/

Table S7C : Chemistry: Two layers of PP mesh with 3-dimentional structure

Code	Sections	SEM 500 X	ATR-FTIR	DSC
DHU13-52	First layer	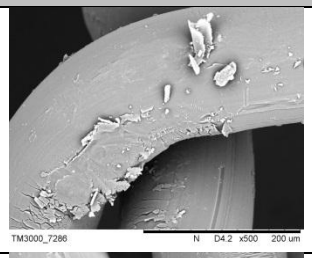	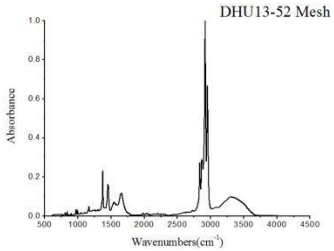	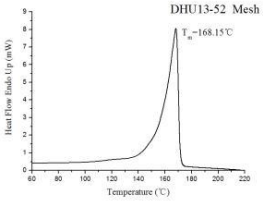
	Second layer	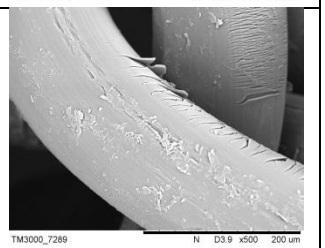		

Table S7D: Chemistry: Single ePTFE membrane

Code	Sections	SEM	ATR-FTIR	DSC
		500 X		
DHU13-11 (1035 days)	Membrane	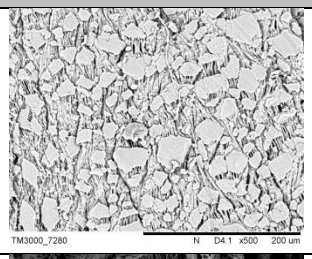	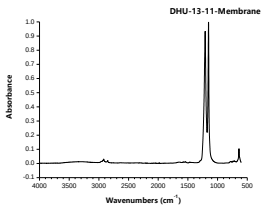	/
		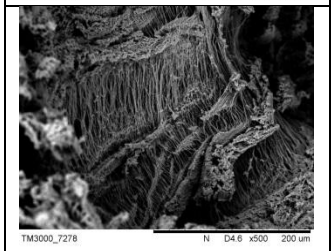		/

Table S7E: Chemistry: One layer of PP mesh + ePTFE membrane

Code	Sections	SEM	ATR-FTIR	DSC
		500 X		
DHU13-13 (558 days)	Mesh	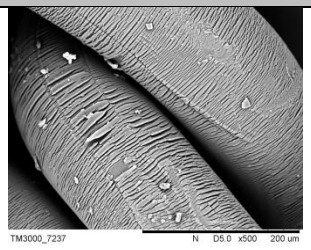	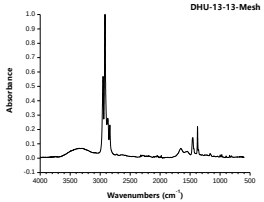	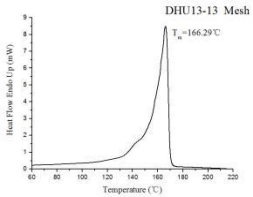
	Membrane	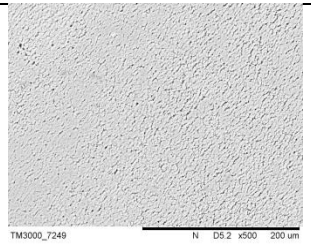	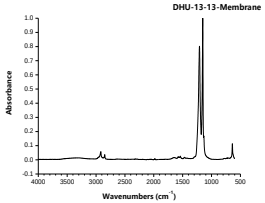	/

Table S7F(A): Chemistry: double-layer of PP + ePTFE

Code	Sections	SEM	ATR-FTIR	DSC
		500 X		
DHU13-2 (1050 days)	First layer	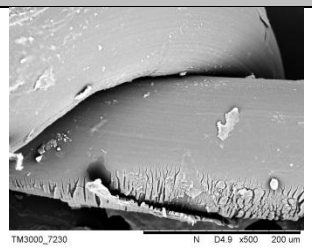	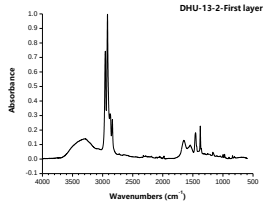	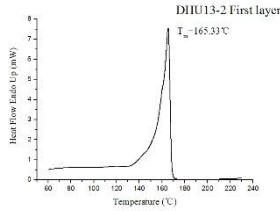
	Second layer	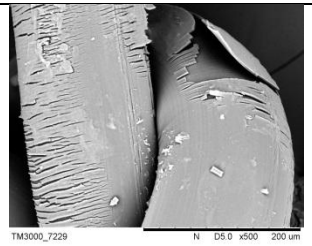	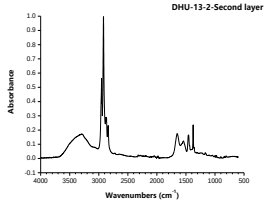	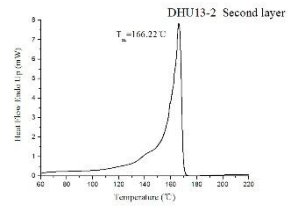
	Membrane	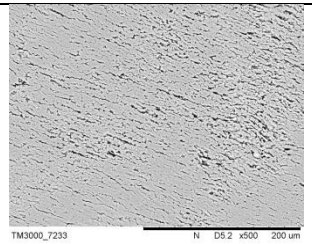	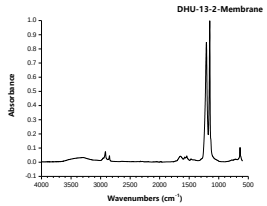	/

Table S7F(B): Chemistry: double-layer of PP+ ePTFE

Code	Sections	SEM	ATR-FTIR	DSC
		500 X		
DHU13-4 (683 days)	First layer	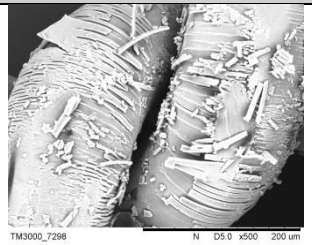	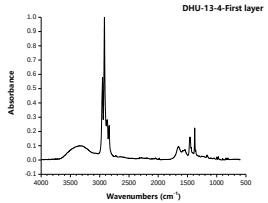	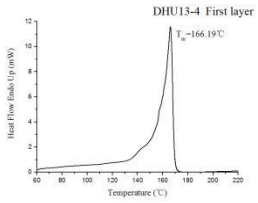
	Second layer	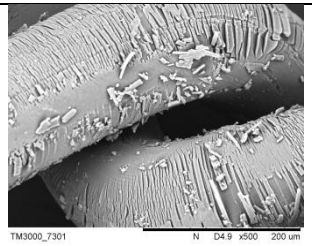	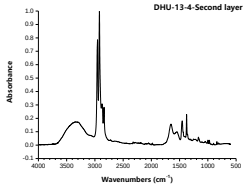	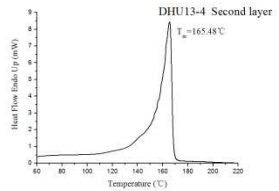
	Membrane	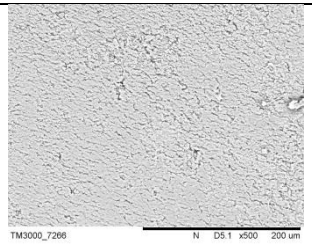	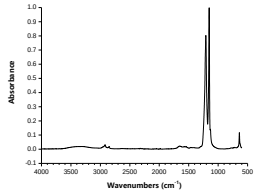	/
	Hole	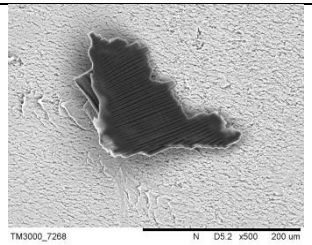	/	/

Table S7F(C): Chemistry: double-layer of PP + ePTFE

Code	Sections	SEM	ATR-FTIR	DSC
		500X		
DHU13-6 (600 days)	First layer	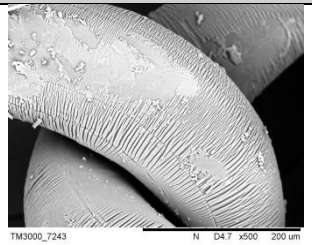	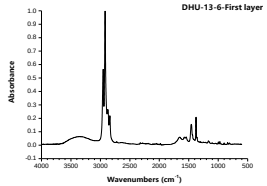	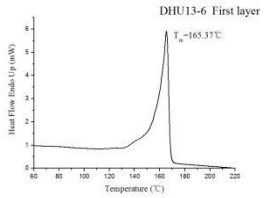
	Second layer	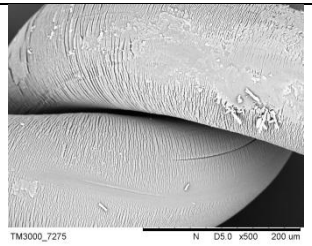	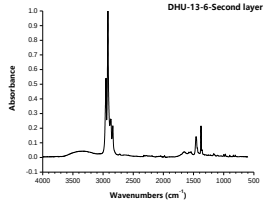	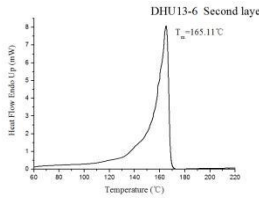
	Membrane	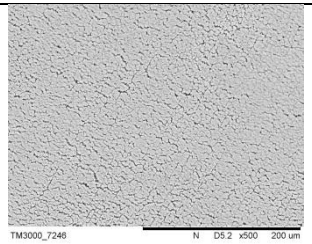	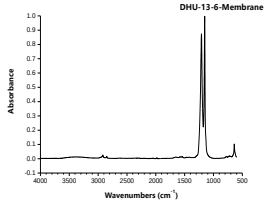	/

Table S7F(D): Chemistry: double-layer of PP+ ePTFE

Code	Sections	SEM	ATR-FTIR	DSC
		500X		
DHU13-57	First layer	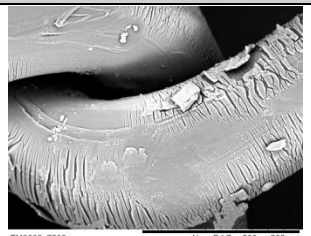	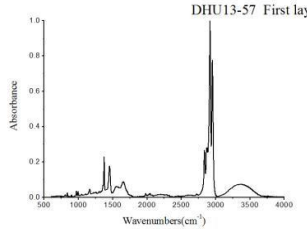	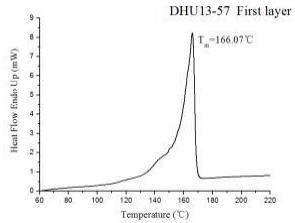
	Second layer	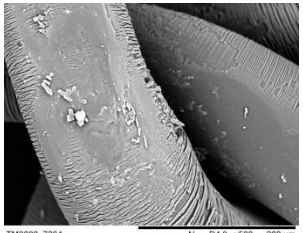	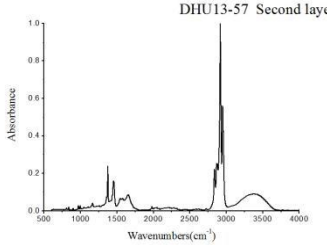	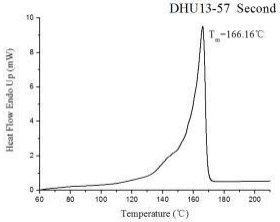
	Membrane	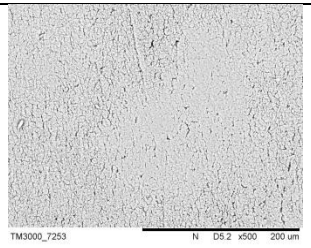 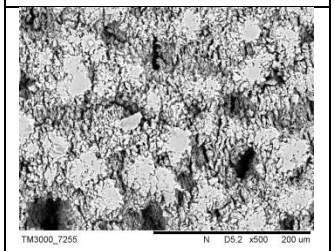	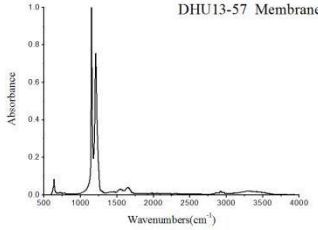	/ /